Organic Matter Composition of Biomineral Flocs and its Influence on Suspended Particulate Matter Dynamics along a Nearshore to Offshore Transect

Michael Fettweis[1], Markus Schartau[2], Xavier Desmit[1], Byung Joon Lee[3], Nathan Terseleer[1], Dimitry Van der Zande[1], Rolf Riethmüller[4]

[1] OD Natural Environment, Royal Belgian Institute of Natural Sciences, rue Vautier 29, 1000 Brussels, Belgium

[2] GEOMAR Helmholtz Center for Ocean Research, Wischhofstr. 1-3, 24148 Kiel, Germany

[3] Department of Advanced Science and Technology Convergence, Kyungpook National University, 2559 Gyeongsang-daero, Sangju, Gyeongbuk 742-711, Korea

[4] Institute of Coastal Ocean Dynamics, Helmholtz Center Geesthacht, Max-Planck-Str. 1, 21502 Geesthacht, Germany

Corresponding author: Michael Fettweis (mfettweis@naturalsciences.be)

Key Points:

- Floc sizes vary as a function of tides and seasons in the high turbid nearshore. In the low turbid offshore floc sizes have mainly a seasonal signal.
- The median floc size increases in the presence of fresh TEP, which is mostly present in spring and summer. Mineral-associated TEP has no detectable influence on the floc size.
- Separation of POC, PON and TEP in fresh and mineral-associated components using a semi-empirical model approach.

24 **Graphical Abstract**

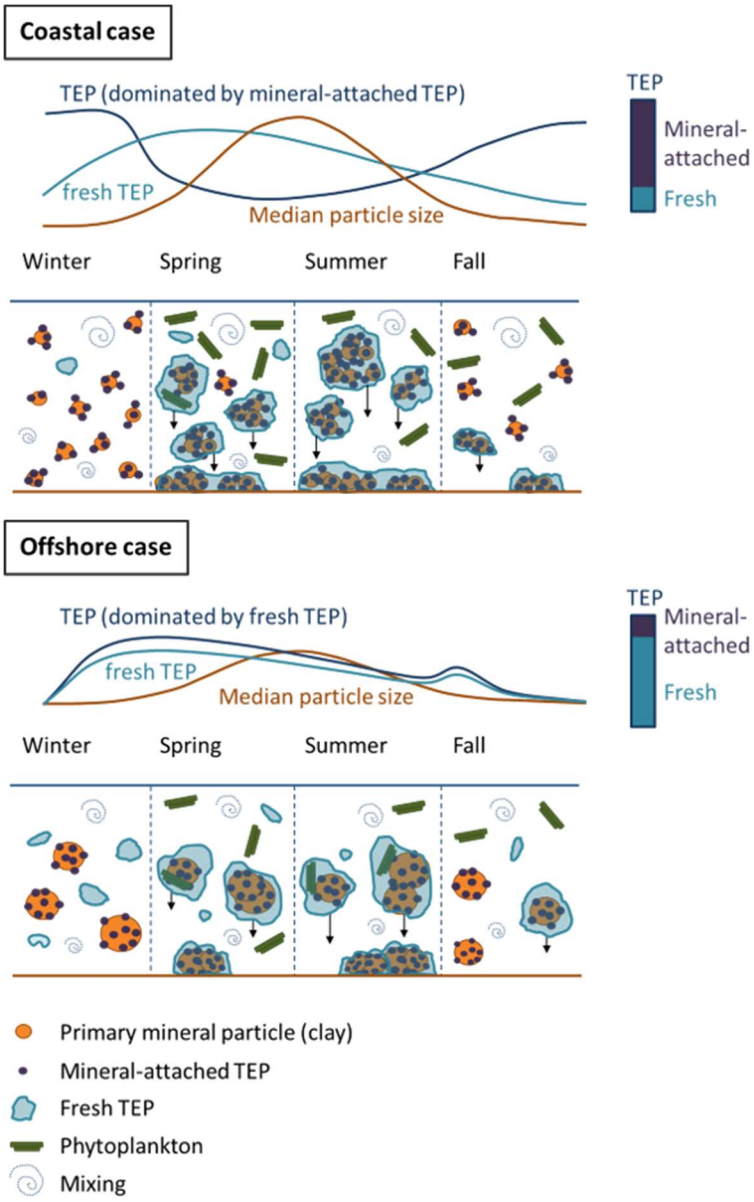

25

26

Abstract

The seasonal variation in concentration of transparent exopolymer particles (TEP), particulate organic carbon (POC) and nitrogen (PON) were investigated together with floc size and the concentration of suspended particulate matter (SPM) along the cross-shore gradient, from the high turbid nearshore towards the low-turbid offshore waters in the southern Bight of the North Sea. The analyses of TEP, POC and PON result in a set of parameters that incorporate labile and refractory organic matter (OM) fractions. Our data demonstrate that biophysical flocculation cannot be explained by these heterogeneous parameters, but requires a distinction between a more reactive labile ("fresh") and a less reactive refractory ("mineral-associated") fraction. Based on the data at all sample stations, we separated the labile and mineral-associated POC, PON and TEP using a semi-empirical model approach. The model's estimates of fresh and mineral-associated OM show that great parts of the POC, PON and TEP are associated with suspended minerals, which are present in the water column throughout the year, whereas the occurrence of fresh TEP, POC and PON is restricted to spring and summer months. In spite of a constantly high abundance of total TEP throughout the entire year, it is its fresh fraction that promotes the formation of larger and faster sinking biomineral flocs, thereby contributing to reduce the SPM concentration in the water column over spring and summer. Our results show that the different components of the SPM, such as minerals, extracellular OM and living organisms, form an integrated dynamic system with direct interactions and feedback controls.

Plain Language Summary

Particles, suspended in coastal waters, occur as loose aggregates of tiny mineral and organic particles, also known as flocs. Their mass concentration is higher in winter than in summer, but their sizes are smaller in winter. The seasonal cycle of phytoplankton activity drives this phenomenon. In spring, phytoplankton blooms and starts to produce fresh and sticky organic matter. This glue binds particles together after collisions and promotes increasingly larger and yet stable flocs. Analytical lab methods cannot distinguish between the freshly produced sticky and the older inactive, mineral bound organic material that is stored in the sediments and entrained into the water by erosion and resuspension. Therefore, previous studies were not able to detect the relation between the occurrence of the sticky material and the floc-sizes in coastal waters. However, our new innovative model approach allows a separation into both fractions. We observe a clear increase in floc sizes during spring and summer when fresh sticky material is available. As larger particles sink faster, they are removed from the waters which allows more light to penetrate. In this way, phytoplankton changes its growth conditions, a nice example how an integrated dynamic system with direct interactions and feedback loops forms.

1 Introduction

Interactions and feedback loops between organic and mineral particles have an impact on sediment dynamics as well as on primary production in nearshore marine ecosystems (Droppo, 2001; Muylaert et al., 2006; Jago et al., 2007; Fettweis et al., 2014; Maerz et al., 2016; Liénart et al., 2017; Neumann et al., 2019; Schartau et al., 2019, Skinnebach et al., 2020; Fall et al., 2021). The suspended particulate matter (SPM) concentration can be highly variable in these areas due to hydrodynamic (tidal currents) and atmospheric (waves and solar radiation) energy entrainment, weather and climate, biological activity and terrestrial export (Schlünz & Schneider, 2000; Pietrzak et al., 2011; Fettweis et al., 2012; Wang et al., 2013), as well as human activities such as trawling, dredging and dumping operations, and major engineering works (e.g. Milliman et al., 1987; Manning et al., 2011; Baeye & Fettweis, 2015). SPM controls marine ecosystems through, for example, its influence on water clarity, filter-feeding animals, mineral and organic seabed composition or as carriers of pollutants (van Hoey et al., 2005; Regnier et al., 2013; Capuzzo et al., 2015; Zhang et al., 2017; Hendriks et al., 2020). The interactions between physical forcing, biological and chemical processes, and human activities result in highly variable spatial and temporal scales of SPM concentration and composition (Eisma & Kalf, 1979; Ittekkot & Laane, 1991; Mayer, 1994; Fettweis et al., 2006; Van Beusekom et al., 2012; Adriaens et al., 2018; Blattmann et al., 2019). SPM is composed of particulate inorganic (PIM) and particulate organic matter (POM). Flocculation processes combine these particles into biomineral flocs (Shen et al., 2018; Lee et al., 2019), which overcompensates the resulting decrease in overall density and therefore yields higher settling velocities compared to most of their individual constituents (e.g. Engel & Schartau, 1999; Mietta et al., 2009). In tidally dominated, mostly shallow environments, floc break-up dominates during periods of high currents and waves with strong shear. In contrast, the formation of larger flocs prevails during slack water periods (e.g. Winterwerp, 1998). The size of the flocs is theoretically determined by the smallest turbulent eddies (Braithwaite et al., 2012). But floc size can exceed those of the turbulent eddies in the presence of biogenic particles whose surfaces can become exceedingly sticky (Cross et al., 2013).

SPM concentration in the North Sea is higher in winter and lower in summer (Howarth et al., 1993). This seasonality appears to be caused mainly by biological cycles and only to a minor part by the higher storm frequencies in winter (Fettweis et al., 2014; Lai et al., 2018). Biological processes influence flocculation, seabed erodibility and transport of the suspended particles, because of the emergence of polysaccharides such as exopolymeric substances (EPS; e.g. Verdugo et al., 2004), including gel-like particles like transparent exopolymer particles (TEP; e.g. Alldredge et al., 1993; Logan et al., 1995) and Coomassie stainable particles (e.g. Long & Azam, 1996). Dissolved EPS are the precursors of these particles and refer to any extracellular dissolved organic matter released from phytoplankton and bacteria, either actively by exudation or passively via viral lysis, sloppy feeding or through bacterial degradation (Passow, 2000; Engel & Passow, 2001; Engel et al., 2020). TEP are known to be a common component of the organic matter (OM) in marine environments, having specific characteristics such as adhesiveness, transparency, flexibility and may form biofilms (Zhou et al., 1998; Passow, 2002; Mari & Robert, 2008).

The interactions between TEP and SPM have mainly been studied in open ocean environments where mineral concentrations are low and the hydrodynamics is weaker than in coastal regions. Typically, under open ocean conditions TEP concentrations are correlated with

the rise and decline of phytoplankton blooms (Fukao et al. 2010; Mari et al., 2017). But for nearshore and estuarine environments TEP data in combination with SPM measurements are scarce. Here, hydrodynamical forces are strong, the SPM dynamics is complex and the mineral fraction of the SPM is dominant. Published data show that in winter, when SPM concentration frequently reaches high values, also concentrations of OM, including TEP, become high, displaying maxima within high turbid areas (Malpezzi et al. 2013; Morelle et al., 2018). Thus, a correlation between total TEP concentration and floc size is inextricable. Extensive mixing events in spring and summer can generate SPM concentrations similar to those found in winter, but with floc sizes that are significantly larger. This apparent contradiction indicates that TEP concentration alone cannot sufficiently explain biophysical flocculation.

The aim of our study is to gain deeper insight into the connection of TEP as a driver of flocculation with the temporal and spatial variation in SPM and floc size dynamics. This is based on numerous water samples collected between 2004 and 2020 in the Belgian part of the North Sea. We investigate the seasonal variations of the interrelation between concentration and OM composition of SPM. Further, we provide insight to unraveling apparent discrepancies in observations with respect to SPM concentration, floc size and the qualitative composition of the particulate organic matter (POM), notably the fresh and labile vs mineral-associated and more recalcitrant fraction. This paper is structured as follows: First, the fresh and mineral-associated POM concentration in the particulate organic carbon (POC), nitrogen (PON) and TEP fractions is differentiated, refining the POM-SPM modelling approach of Schartau et al. (2019). Then, the seasonality of the size and density of biomineral flocs along the coastal to offshore gradient, using in situ data, is related to fresh and mineral-associated POM. Finally, the model is applied to estimate fresh and mineral-associated POM from in situ and satellite SPM measurements to discuss the temporal and geographical variability of SPM concentration and composition across the onshore-offshore gradient.

2 Methods

2.1 Measuring Strategy

2.1.1 Water and Seabed Samples

Water samples were taken in the Belgium part of the North Sea from March 2018 until July 2020 at three locations along a cross-shore section (MOW1, W05 and W08; Figure 1). It ranges from the nearshore coastal turbidity maximum (MOW1) to the offshore under complete Channel water influence (W08). W05 is located in between at the outer margin of the coastal turbidity maximum. Lacroix et al. (2004) deduce from model tracer experiments backed-up by long-term salinity observations that at W05 and MOW1 Channel waters still dominate and that at MOW1 fresh waters from the Rhine-Meuse and the Scheldt contribute with about 6%. The present-day SPM in the Belgian-Dutch nearshore area originates mainly from the erosion and resuspension of the existing mud deposits situated in the Belgian nearshore and the present-day Scheldt estuary can be excluded as source of fine-grained sediments (Adriaens et al., 2018).

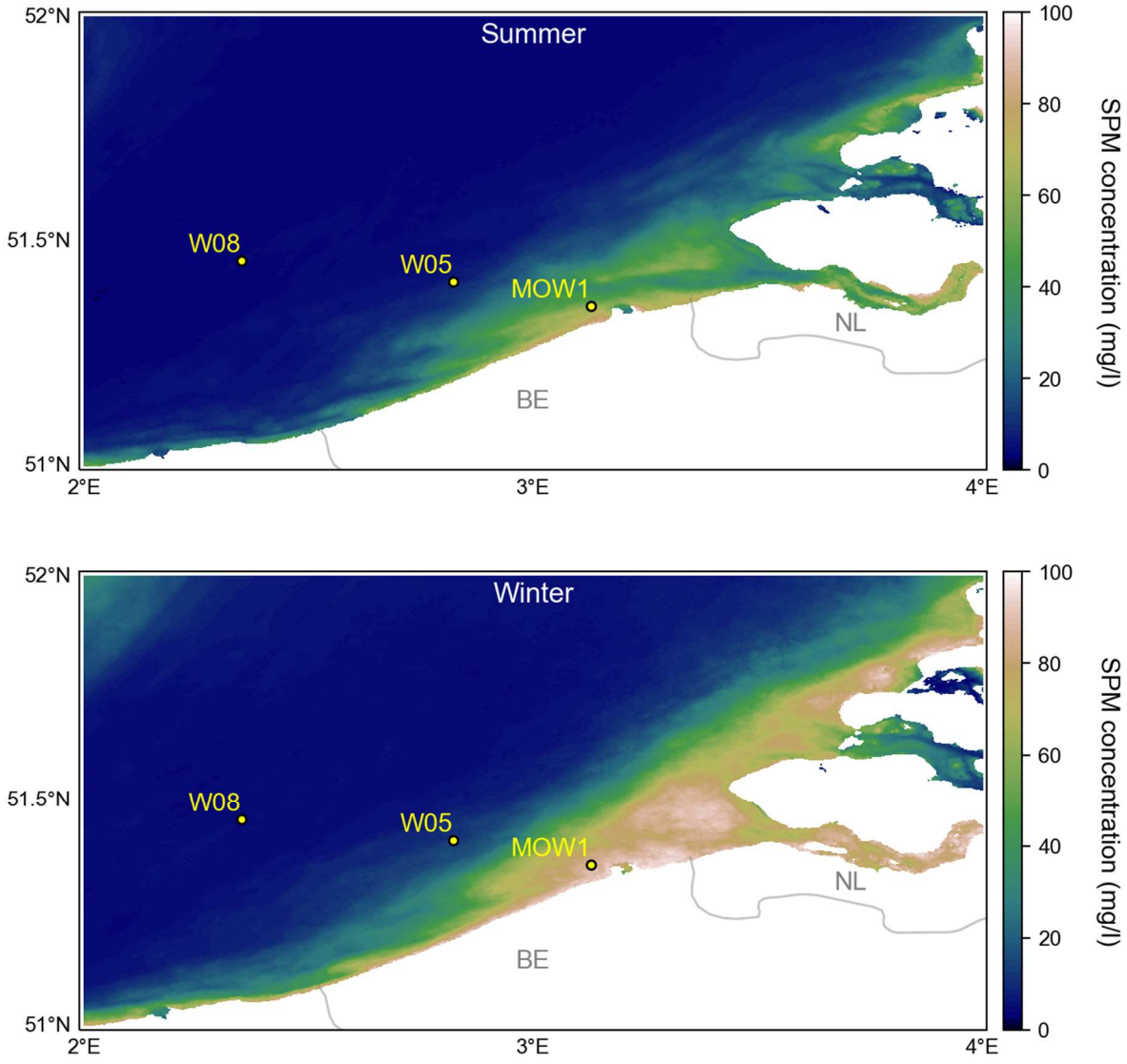

Figure 1: Map of sampling stations MOW1, W05 and W08 (BE: Belgium, NL: The Netherlands). The background displays the averaged near surface SPM concentrations in the Belgian coastal zone (southern North Sea) computed from satellite images taken by Sentinel-3/OLCI from April 2019 to September 2019 (above) and from November 2019 to March 2020 (below).

Sampling was carried out every 1 or 1.5 hours during a tidal cycle (12.5 hours) at 2 m below the surface and about 2 m above the seabed using 5 l Niskin bottles attached to a rosette CTD system. During this period about 6 Van Veen grab samples have been taken in each station for the analysis of POC and PON content in the <63 µm fraction. In total 17 tidal cycles have been sampled at the nearshore station MOW1, 10 at the intermediate station W05, and 9 at the offshore station W08. The water samples were filtered on board and analyzed in the laboratory to obtain the concentration of SPM, POC, PON, pigments (Chlorophyll-a: Chl-a; Pheophytin-a: Pheo-a) and, from December 2018 onward, TEP. The Particulate Organic Matter (POM) content was determined by loss-on ignition until November 2019. The sample turbidity (in FNU) was

159 measured with a Hach TL2360 LED Turbidimeter and salinity was analyzed from the water
160 samples. Samples for dissolved inorganic nutrients and Dissolved Organic Carbon (DOC) were
161 taken from the filtrate. From 2004 until 2011, 25 tidal cycle measurements of SPM, POC, PON,
162 and from 2012 until March 2018, 25 additional cycles including pigment concentration have
163 been sampled at station MOW1. During the period March 2004 to March 2018, 7 tidal cycles
164 have been sampled at two offshore stations, in the intermediate zone and 18 in the high turbidity
165 zone for SPM, POC, PON and pigment (the latter from 2012 onward) concentration. The
166 sampling strategy was different before March 2018 as samples have only been taken at about 2 m
167 above the bed and not at the surface. The total amount of samples collected with at least SPM
168 and POC concentration amounts to 1841; the other parameters have respectively 1663 (PON),
169 1810 (Chl-a), 1716 (Pheo-a), 1414 (Salinity), 935 (Hach turbidity) and 659 (TEP) good data.

170 *2.1.2 Sensor Measurements*

171 A LISST 100X was attached to the rosette to measure volume concentrations in 32
172 logarithmically spaced size groups over the range of 2.5–500 μm using laser diffraction
173 (Agrawal & Pottsmith, 2000). Long-term measurements with a LISST 100X and an OBS are
174 available at the station MOW1 from tripod deployments over the period 2005-2019. In the
175 beginning, the tripod was moored for 3 to 6 weeks and then recovered. From December 2009 an
176 advanced tripod system allowed continuous time series. The LISST 100X was mounted at 2 m
177 above bed (mab) and the OBS at 0.2 and 2 mab. In total about 1716 days of "good" LISST data
178 have been collected and about the double of "good" OBS data. "Good" LISST data are defined
179 by a smooth (i.e., no sudden decrease) optical transmission within a range between 0.15 and
180 0.98, a smooth floc size distribution (FSD) and no biofouling. The latter two disturbances have
181 regularly been observed in the long-term data series. Disturbed FSDs occur when the laser beam
182 is misaligned. Biofouling occurs mainly in spring and summer and is identified by a gradual
183 decrease in transmission or optical backscatter and increase in SPM volume concentration. OBS
184 data have been discarded when the sensor output changed over time unrelated to changes in
185 inherent particle properties or SPM concentration. This was caused by variations in voltage
186 supply, changes in the transmittance of the window that is the interface between the sensor and
187 the water and the signal was attenuated by biofouling (Fettweis et al., 2019). The OBS output has
188 first been calibrated against a laboratory standard (AMCO clear) in order to convert the sensor
189 output to a backscatter turbidity unit, before being calibrated in situ with SPM concentration
190 derived from water samples in order to obtain a mass concentration.

191 *2.1.3 Remote Sensing Measurements*

192 Surface SPM and Chl concentration have been derived from the Ocean and Land Color
193 Instrument (OLCI). OLCI is a multispectral radiometer carried on board Sentinel-3A (launched
194 in 2016) and B (launched in 2018) with 21 bands on the 400-1200 nm spectral range and a
195 spatial resolution of 300 m. The two satellites provide a daily revisit time over the southern
196 North Sea. Sentinel-3/OLCI baseline water products (L2-WFR) were retrieved from the
197 Copernicus Online Data Access (CODA) service hosted by EUMETSAT (coda.eumetsat.int).
198 The baseline products were processed with IPF-OL-2 version 06.13 (EUMETSAT, 2019) with
199 standard masking applied, i.e. excluding INVALID, LAND, CLOUD, CLOUD_AMBIGUOUS,
200 CLOUD_MARGIN pixels. Additionally, a custom quality control was applied to remove outlier
201 pixels with a spectrally flat signal. The SPM product was generated by an artificial neural
202 network as a multiple non-linear regression technique to deal with the optically complex waters

in the study area. The artificial neural network, originally developed by Doerffer and Schiller (2007), was updated to become the Case 2 Regional (C2RCC) processor suitable for Sentinel-3 (EUMETSAT, 2019). Generating reliable satellite estimates of Chl-a in optically complex coastal waters is still challenging. Many algorithms exist and give quite different performance for different optical conditions. For this reason, we applied the approach of Lavigne et al. (2021) who clearly defined the limits of applicability of three popular and complementary algorithms: 1. the OC4 blue-green band ratio algorithm which was designed for open ocean waters; 2. the OC5 algorithm which is based on look-up tables and corrects OC4 overestimation in moderately turbid waters; and 3. a near infrared-red (NIR-red) band ratio algorithm designed for high turbid waters. This approach allows automatic pixel-based switching between the most appropriate algorithms for a certain water type. For the measuring stations these are depending on the season, OC4 and OC5 for W08, OC5 and NIR-red for W05 and NIR-red for MOW1.

2.2 Sample and Data Analysis

2.2.1 Water Samples

At every sampling occasion, three subsamples for SPM concentration were taken and filtered on board using annealed (24 hours in a muffle furnace at 400°C) and pre-weighted 47mm GF/C filters. The filters were then rinsed with MilliQ water and immediately stored at -20°C, before being dried during 24 hours at 50°C and weighted to obtain the concentration. The absolute detection limit is 0.4 mg and the uncertainty (expressed as the RMSE of the triplicates divided by the mean value) decreases with increasing concentration from 8.5% (SPM concentration < 5 mg/l) to 6.7% (<10 mg/), 3.5% (10–50 mg/l) and 2.1% (>100 mg/l) and represent the random error related to the lack of precision during filtrations. Especially in clearer water, systematic errors due to the offset by salt or other errors become much larger than the random errors (Neukermans et al., 2012; Fettweis et al., 2019). These are not included, and have been estimated based on Stavn et al. (2009) and Röttgers et al. (2014) as 1 mg/l. One of the SPM filters was used to determine the POM content, through Loss-on-Ignition (LoI) in a muffle furnace at 500°C during a few hours and reweighting. The samples for POC and PON were filtered on board using 25mm glass fiber filters, stored immediately at -20°C and analyzed in the laboratory through catalytic oxidation and gas chromatography using a FLASH EA 1112 – Element analyzer. The analytical uncertainty for POC and PON are 12% and 18% and the detection limits 0.018 mg/l and 0.009 mg/l respectively. The sample for pigment concentration was filtered on 47mm GF/C glass fiber filters, stored in liquid Nitrogen and determined in the lab using ultra high-performance liquid chromatography. The analytical uncertainty for Chl-a and Pheo-a is 23% and 31% and the detection limits are 0.023 µg/l and 0.015 µg/l. We added to these analytical uncertainties the random errors due to filtration, which we assumed to be equal to the ones of SPM concentration. The method for TEP analysis follows the one described in Nosaka et al. (2017). This method is, as many other semi-quantitative methods, based on Aldredge et al. (1993) and Passow and Aldredge (1995). Three subsamples for TEP concentration have been taken and filtered using 25mm 0.4 µm polycarbonate filters with low under-pressure. The filters have been colored immediately after filtration with 1 ml of Alcian blue, rinsed with 1 ml of MilliQ water and stored at -20°C. The stained particles are related to a weight equivalent for the anion density of TEP and standardized using xanthan gum (Passow and Alldredge, 1995; Passow 2002). The units for TEP are expressed as mg xanthan gum equivalents per liter (mg XG eq./l). The filtrates were collected in sample tubes for DOC, inorganic nutrients and analyzed using

standard spectrophotometric methods with a Skalar autoanalyzer. The detection limit for DOC is 0.09 mg C/l.

2.2.2 Sediment Samples

The POC and PON content of the bed surface samples was determined for the fraction < 63 µm using the same method as described above.

2.2.3 Floc Size Distribution and Effective Floc Density

The volume concentration of each size class is used to build the floc size distributions (FSD), and thus the median floc size (D50) and total SPM volume concentration are computed from the FSDs. The uncertainties and limitations of the LISST 100X detectors are related to the shape, size and inherent optical properties of the particles occurring in nature, and to the measuring principle (Mikkelsen et al., 2006; Andrews et al., 2010; Davies et al., 2012; Schwarz et al., 2017) and will influence the FSD. In case of a too low turbidity (transmission >90%) the data becomes less accurate. The diameter of a particle is an exact proxy of its size if the particle is a sphere. Natural particles, such as flocs, have irregular shapes and generally follow Junge or multimodal log-normal distributions (e.g. Liley, 1992; Buonassissi & Dierssen, 2010). Measurements by laser diffraction result thus intrinsically in a particle size distribution that is generally lognormally distributed. The effective floc density (ρ_{eff}) is the ratio of floc mass (M_f) over floc volume (V_f) minus the water density (ρ_w). The floc mass, M_f, can be calculated as:

$$M_f = M_p + M_w = M_p + \rho_w (V_f - V_p) = M_p + \rho_w (V_f - M_p / \rho_p) \quad (1)$$

where ρ_p is the primary particle density, M_w is the mass of water and M_p the mass of primary particles in the flocs. The latter can be obtained from the SPM filtrations, the water density was fixed at 1025 kg/m³, the primary particle density was estimated as 2500 kg/m³ (Fettweis, 2008) and the floc volume is the volume concentration measured by the LISST.

2.2.4 Long-Term Measurements of the FSD and SPM Concentration

The structure of the long-term FSD time series at MOW1 has been investigated using the entropy analysis (e.g. Mikkelsen et al., 2007). Applied to FSDs, entropy analysis allows grouping the size spectra without assumptions about the shape of the spectra. It is therefore suited to analyze unimodal as well as multimodal distributions. Firstly, the 60 minutes averaged FSD time series were normalized by dividing each of the 32 size classes by the total volume concentration of the FSD and then pl64 low-pass filter (Beardsley et al., 1985) removed the tidal signal. Next, a climatological FSD over the period 2006-2019 was generated by averaging the data of each time stamp related to the start of the respective year. Finally, a climatological entropy classification was carried out using the FORTRAN routine of Johnston and Semple (1983). In accordance with Fettweis et al. (2014) four entropy groups have been chosen for the classification. The pl64 low-pass filter was also applied to the long-term SPM concentration time series before a climatological SPM concentration was calculated over the period 2005-2016 similar as the climatological FSD time series.

2.3. Model Based Differentiation of OM between Fresh and Mineral-Associated Fractions

The inorganic and organic components of the SPM have different origins. The mineral particles may have a detrital or biogenic origin. The detrital PIM typically incorporates clays, quartz and other minerals, while biogenic PIM consists of minerals such as carbonates and amorphous silicates. In the further considerations, we will only consider PIM as a whole. The POM is a mixture of compounds derived from marine photosynthesis or terrestrial sources. It is a combination of diverse detrital organic substances as well as of living organisms such as bacteria, phyto- and zooplankton. The POM can be refractory, mineral-associated, or fresh. The first two have a low susceptibility and the last one a high susceptibility towards microbial degradation (Arndt et al., 2013). We will use the adjectives 'mineral-associated' (POM_m) for the more recalcitrant and 'fresh' (POM_f) for the labile and semi-labile fraction. The POM_m is incorporated in the mineral fraction where it is particularly bound with clay minerals (Mayer, 1994).

2.3.1 Model Assumptions

For the differentiation between the POM_f and POM_m we follow the approach of Schartau et al. (2019), who considered Loss-on-Ignition (LoI) measurements for describing the POM:SPM ratio as a function of SPM concentration using a semi-empirical model. The conceptual basis of the POM-SPM model is that the POM concentration can be written as the sum of the POM_f and POM_m concentrations and that POM_m is assumed to be linearly correlated with the PIM concentration by a constant proportionality factor m_{POM}:

$$POM = POM_f + POM_m = POM_f + m_{POM}\, PIM \tag{2}$$

The assumption is that the seasonal built up of fresh POM (POM_f) can be described as a saturation function of the SPM concentration:

$$POM_f = \frac{K_{POM}}{\frac{K_{POM}}{SPM}+1} \tag{3}$$

with the parameter K_{POM} (in the same units as SPM concentration) being the second parameter of the POM-SPM model. The function reaches a saturation at high SPM concentrations where POM_f equals K_{POM}, while at low SPM concentration POM_f concentration tends to zero. This approach assumes that the production of POM_f is eventually limited by nutrients, temperature and light availability. Optimized values of K_{POM} were shown to be subject to seasonal variations, whereas values estimated for m_{POM} turned out to be fairly constant and independent of seasonal conditions (Schartau et al., 2019). According to the POM-SPM model, the POM content of SPM can be approximated by:

$$\frac{POM}{SPM} = \frac{POM_f}{SPM}\frac{1}{m_{POM}+1} + \frac{POM_m}{SPM} \tag{4}$$

A non-linear dependency between POM content and SPM concentration is obtained by including eq. (3) in eq. (4). The combined equation has some meaningful and desired convergence characteristics. For SPM concentration approaching zero, POM content converges to 1 (and POM_f fraction dominates POM) and for high SPM it approaches $\frac{m_{POM}}{m_{POM}+1}$ (and POM_m fraction dominates POM). Instead of using LoI data for POM content, we considered three different types of organic matter data, namely the concentrations of POC, PON, and TEP. The POM-SPM

model was refined by introducing two parameters (f_1 and f_2) for every observational type X_i (POC, PON, and TEP) to the POM-SPM model (Eq. 5):

$$\frac{Xi}{SPM} = f_{1,X_i}\frac{POM_f}{SPM}\frac{1}{m_{POM}+1} + f_{2,X_i}\frac{POM_m}{SPM};\ \mathrm{X_i}\ [POC, PON, TEP]; \qquad (5)$$

These additional parameters $f_{1,Xi}$ and $f_{2,Xi}$ represent relative proportions of X_i to POM, e.g. $f_{1,X2}$ and $f_{2,X2}$ express the ratios of fresh- and of mineral-associated PON to POM (or $f_{1,X1}$ and $f_{2,X1}$ for respective ratios of POC to POM) in units of molecular weight (g g^{-1}) or TEP to POM in units of (g XG eq.)/(g POM), respectively. In this manner, consistent and meaningful estimates of $f_{1,Xi}$ and $f_{2,Xi}$ could be derived. Values assigned to or estimated for K_{POM} and m_{POM} should be largely independent of the observational type, no matter whether POC, PON, or TEP concentrations are considered. Overall, the refined model requires values to be assigned to four parameters (m_{POM}, K_{POM}, f_1 and f_2). Consequently, and somewhat different from the POM:SPM model, the respective fraction of X_i converges to $f_{1,Xi}$ at SPM concentration approaching zero. For high SPM concentrations the portion X_i of SPM approaches $f_{2,X_i}\frac{m_{POM}}{m_{POM}+1}$.

2.3.2 Parameter Optimization

The mineral-associated POM_m of the SPM is entirely determined by the value assigned to the parameter m_{POM} (eqs. 2 and 4). The parameters m_{POM} and f_2 are collinear and therefore they cannot be estimated independently. For maintaining consistency between the previous parameter estimates of m_{POM}, and the added parameters of f_2 ($f_{2,POC}$, $f_{2,PON}$, and $f_{2,TEP}$) we used the optimized value (m_{POM} = 0.13) of Schartau et al. (2019). This estimate was obtained by using data of all seasons within the German Bight and German part of the Wadden Sea in the south-eastern region of the North Sea. The uncertainty of this estimate for m_{POM} is small (<3%) and the seasonal variations between estimates turned out to be small as well (0.12 - 0.14). With a fixed value assigned to m_{POM} we only require values of three parameters to be optimized. The values of f_1, f_2, and K_{POM} were estimated by minimizing the negative logarithm of a likelihood and a prior (cost function) that was used as a metric for assessing the deviation between observational data and the model counterparts. In general, for the likelihood (description of the data, given the model) and prior (deviation between estimated and some prescribed characteristic parameter value) we assumed respective probability densities to be normal, represented as Gaussian functions of the data-model residuals and of the deviation of parameter estimates from a prior value assigned to K_{POM}. Reasons for why we had to account for prior information will be explained in the following paragraph. We explicitly accounted for uncertainties in the observations and in the prior value of K_{POM}. Optimal combinations of parameter values were determined for seasonally sorted data sets of POC, PON, and TEP. The observational data reveal pronounced variability at low SPM concentrations, which becomes much reduced at high SPM concentrations. At high SPM concentrations (>100 mg/l), uncertainties in measurements were much lower than the variations due to spatio-temporal variability. Like in the approach of Schartau et al. (2019), we added the variance of the observed POC:SPM, PON:SPM, and TEP:SPM to the measurement uncertainties for SPM concentrations >100 mg/l, otherwise individual data points at such high SPM concentrations can introduce severe biases in the estimates of the parameters f_1 and K_{POM}. For all data points we calculated variances for POC:SPM, PON:SPM, and TEP:SPM, following the law of error propagation, based on individual measurement errors of SPM, POC, PON concentrations. Errors for TEP were assumed

to be 15% of the measured concentrations, which was approximately the highest relative error found for the POC concentration measurements.

The cost functions' minima yield the best model representations of the POC:SPM, PON:SPM, and TEP:SPM data. Respective minima (best parameter values) were identified by exploring the parameter space including combinations of the three parameters of interest, f_1, f_2, and K_{POM}. Intervals and resolution differed between the observational types for f_1 and f_2. For POC and TEP we chose f_1 and $f_2 \in [0.01,1]$ with a resolution of $\Delta=0.01$ (with 100 elements respectively). For PON we had to increase the variational range and resolution for $f_1 \in [10^{-3},1]$ (resolution $\Delta=10^{-3}$) as well as for $f_2 \in [5x10^{-4},1]$ ($\Delta=10^{-4}$). Possible values of KPOM span two orders of magnitude and we therefore assigned a constant resolution on logarithmic scale (Δlog=5x10-3) within the interval $\log_{10}(K\text{POM}) \in [\log_{10}(0.1), \log_{10}(10)]$, which approximates a precision of 1%. The parameter screening is fast enough for deriving confidence intervals of respective parameter estimates via subsampling. A range of best parameter estimates was confined from 100 individual optimizations, based on random data subsamples that each included 30% of respective total data points. Doing so we learned that estimates of f_1 can become poorly constrained (mainly when using autumn data) for some subsamples that yield estimates of $K_{POM} < 0.5$ mg/l. By introducing an additional term as a prior to the likelihood-based cost function, the optimization problem became well-posed for all subsample cases and we could obtain robust parameter estimates. For the prior we imposed a K_{POM} value of 2.0 mg/l, with a 100% uncertainty (=2.0 mg/l) for all seasons apart from autumn, for which we had to prescribe a 25% uncertainty (=0.5 mg/l) for the prior. Based on the 100 individual optimizations, each with a different set of subsampled data, we determined statistical properties of the estimates, including lower and upper limits of 95% confidence intervals respectively. Instead of the arithmetic mean, the median of the parameter estimates turned out to be a better representation of the overall model fit to the data. This is because curved collinearities appeared in few cases and respective mean values did not coincide with the curved (banana-shaped) spread of optimal parameter values. In all other cases the median was similar to the mean of the estimates.

For model descriptions of POC:SPM and PON:SPM we considered seasonal variations and distinguished between in parameter estimates accordingly, combining data from three months: winter (December, January, and February), spring (March, April, and May), summer (June, July, and August), and autumn (September, October, and November). Monthly parameter estimates were elaborated for model fits to TEP:SPM data. Instead of using data from a single month, we included data from the two adjacent months. For example, optimal parameter values for January were constrained with data from December, January, and February. Likewise, in June the parameter estimates were determined with data from May, June, and July. We recommend such a procedure, because it facilitates the identification of gradual temporal changes in parameter estimates, similar to the low-pass filtering of a moving average.

3 Results

3.1 Temporal and Spatial Variabilities

Some of the measured data together with some physical parameters are shown in Figure 2. The tidal amplitude (Figure 2a) is for Zeebrugge and has been calculated from harmonic analysis, the significant wave height is from a wave buoy near MOW1 (Figure 2b) and has been downloaded from the Measurement Network Flemish Banks (https://meetnetvlaamsebanken.be)

and the daily solar radiation at Zeebrugge (Figure 2c) has been obtained from the Royal Meteorological Institute (https://www.meteo.be). The dissolved and particulate matter data have been averaged over the measuring period (usually 12 hours) and over the vertical. The data averaged over four seasons for all available parameters (2004-2020) are given in the tables in Appendix A. For completeness these tables comprise also parameters that are not further discussed in this study. Variations in parameters occur at tidal, lunar and seasonal scales. Winter (December - February) is the period with low solar radiation, high nutrient concentration and low primary production. In spring (March - May) increasing solar radiation and temperature initiate phytoplankton blooms under nutrient replete conditions. Summer (June-August) has the highest solar radiations (Figure 2c) and nutrients are largely consumed. In late summer - early autumn, a second phytoplankton bloom shows up, but from autumn (September-November) on phytoplankton activity ceases with the decreasing solar radiation and nutrients pile up again. It is interesting to note that for the majority of parameters the more offshore stations W05 (red) and W08 (blue) displayed the same overall course as in MOW1 (black) but with lower values and a lower seasonal variability. Exceptions are median floc size and salinity. Observed variability during a tidal cycle is also less pronounced in the offshore stations. The water column was well mixed in all stations, the variations in salinity between them are, in accordance with Lacroix et al. (2004), caused to a large part by different freshwater contributions from the Rhine-Meuse and the Scheldt rivers. Temperature varied during 2019 sampling between 6.0°C at MOW1 in January (6.3°C at W05, 8.7°C at W08) and 19.9°C in June (19.5°C at W05, 18.2°C at W08). At each station, the highest SPM concentrations occurred in winter and the lowest in summer (Figures 1 and 2d) . The volume SPM concentration has a nearly 75% more pronounced seasonality than the mass SPM concentration (Figure 2d, 2e and *Table A.1-3*). The lower spring-summer volume SPM concentrations correspond to larger floc sizes (Figure 2f) and also to lower effective floc densities (Figure 2g). Median floc size increased towards offshore by about 2. POC and PON concentrations (Figure 2h and 2i) are correlated with SPM concentrations, although higher POC:SPM and PON:SPM ratios occurred during the spring phytoplankton bloom (see Tables in Appendix A). The yearly mean value of the POC/PON ratio is 6.61 molC $molN^{-1}$, practically equal with the Redfield ratio (6.62 molN $molC^{-1}$). Lower values occur in spring (6.37) and summer (6.06) and higher ones in winter (7.01) and autumn (6.75). According to Frigstad et al. (2011), this seasonal variation reflects variations in the water mass characteristics, nutrient concentrations, biomass and OM composition. TEP concentration (Figure 2j) at MOW1 varied between 0.31 and 17.2 mg XG eq./l in winter, 0.62 and 17.57 mg XG eq./l in spring and 1.53 and 6.97 mg XG eq./l in summer. At W05 these values were between 0.11 and 3.31 mg XG eq./l (winter), 0.76 and 4.13 mg XG eq./l (spring) and 0.61 and 1.74 mg XG eq./l (summer); and at W08 between 0.10 and 0.59 mg XG eq./l (winter), 0.52 and 1.09 mg XG eq./l (spring) and 0.28-1.60 mg XG eq./l (summer). The seasonal variation in TEP concentration was similar to POC, PON and SPM concentration and all were somewhat opposite to the DOC concentration (Figure 2k). Although patchy, DOC concentration had generally higher values in summer than in winter, which is explained by the production of DOC by phytoplankton in spring and summer and the subsequent slow degradation (Van Engeland et al., 2010). Chl-a concentration (Figure 2l) was highest during the spring phytoplankton bloom. Except for the spring plankton bloom, the Chl-a concentration at MOW1 was higher than in the offshore stations. This is probably due to the higher availability of nutrients, in spite of the lower water clarity. The winter Chl-a concentrations reached values of a few µg/l in winter, and were thus of the same order of magnitude or even higher than the offshore concentrations in spring and summer. Pheophytin is

one of the breakdown products of chlorophyll and is thus an index of decomposable organic matter (Fuchs et al., 2012). The Pheo-a concentration had an opposite, although weaker, seasonal pattern than the Chl-a concentration. Inorganic nutrient concentrations (for example total dissolved nitrogen, total dissolved phosphate and silicates, see Tables in Appendix A) showed the typical pattern of the North Sea with relatively high concentrations in winter and low concentrations in summer due to nutrient utilization by phytoplankton (Lancelot et al., 2005).

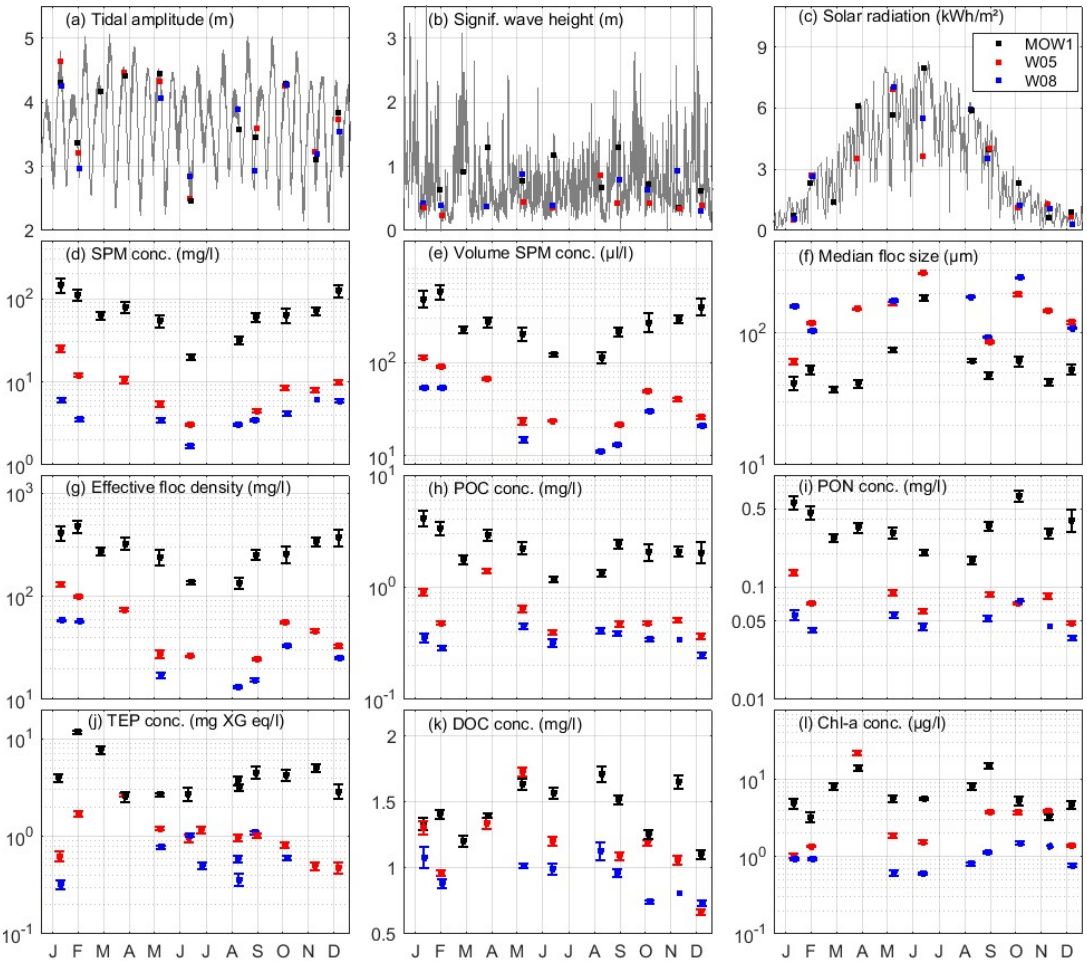

Figure 2: Physical (harmonic tidal amplitude, significant wave height, solar radiation) parameters and dissolved and particulate matter parameters from 2019 (TEP is from 2019 until August 2020) versus time (see § 2.1.1). For the latter, geometric means over the tidal sampling period are shown with their standard errors of the mean in the three sampling stations (MOW1: black, W05: red, W08: blue).

3.2 Floc Size

The hourly floc size distributions measured during a tidal cycle are shown in Figure 3 for the three stations for a winter, summer and autumn month. Common to all, are the tidal changes in volume concentration as a result of deposition, resuspension/erosion and advection. The FSDs at MOW1 were more variable during a tide than at W05 and W08, meaning that break-up and aggregation are dominating the FSD. At W05 and W08, the particles in suspension were not changing significantly in size. This points to strong aggregates and particles of biological origin

that are not subject to turbulence-driven flocculation processes. In spring and, to some extent, in autumn, the FSD at MOW1 became bimodal, with a main peak around 60 µm and a second one around 300 µm. The latter is an indication of the occurrence of large biomineral flocs (Shen et al., 2018). The FSDs at W05 and W08 were unimodal in spring with a peak at 300 µm. In early autumn (September) and in winter they became bimodal, with a secondary peak at around 70 µm (winter) or 100 µm (early autumn). The winter FSD at W05 was more variable as it is located at the edge of the turbidity maximum zone. When the turbidity is higher, then the FSD resembles that of MOW1, in the opposite case it is similar to the offshore station W08 (the latter is shown in the figure). The low-pass filtered median floc sizes from the long-term LISST measurements (2016-2019) at MOW1 are shown in Figure 4. The median floc size is about 50 µm in winter and increases up to 150 µm in summer. The four-class entropy analysis and the associated mean FSD show a mirrored evolution over the year as a function of seasonal changes. The FSD of class 1 (D50 = 47 µm) are most prominent between about 15 October and 15 March, those of class 2 (D50 = 60 µm) in the transitional periods characterized by an increase (15 March to 15 April) or decrease (15 September to 15 October) of biological activity. Class 3 (D50 = 81 µm) and 4 (D50 = 116 µm) prevail over spring and summer. The large biomineral flocs (>200 µm) are more frequent from late spring till early autumn during the decaying phytoplankton blooms, as indicated by the course in Chl-a.

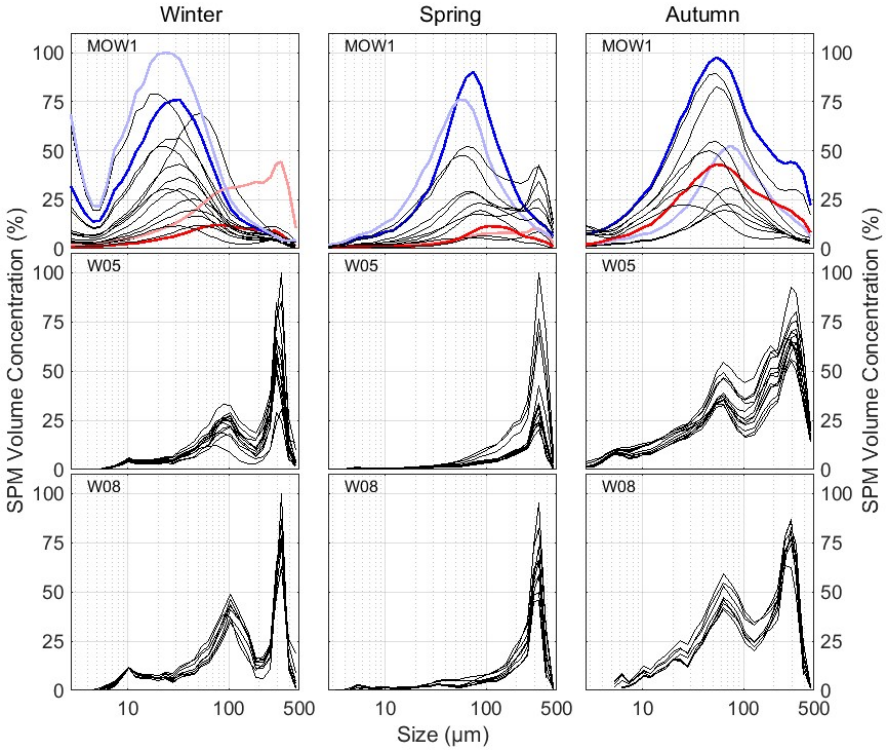

Figure 3: Hourly particle size distribution at about 2 m above the seabed during a tidal cycle at stations MOW1 (January, May, September), W05 (December, May, September) and W08 (December, May, September). The volume concentration is normalized by dividing all values with the largest one measured during the tidal cycle. FSD at MOW1 are highlighted around maximum flood currents (light blue), HW slack (light red), maximum ebb currents (blue) and LW slack (red).

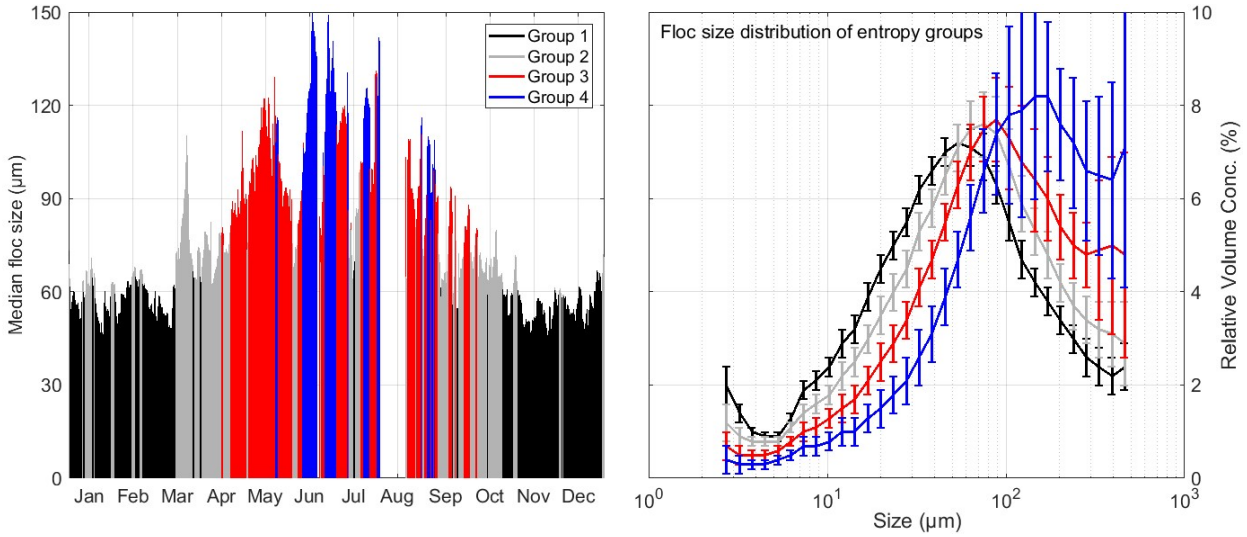

Figure 4: Mean of the low-pass filtered median floc sizes from the long-term LISST measurements (period 2007-2019) at MOW1 (left). The colors indicate the four entropy groups, the corresponding floc size distributions are shown in the right panel.

3.3 Particulate Organic Matter Content of the SPM

The POC and PON fractions of SPM as a function of SPM concentration are shown in Figure 5. The graphs indicate an increase of the OM content with decreasing SPM concentration, which has been documented as a characteristic feature (e.g. Eisma & Kalf, 1987; Jago et al., 1994; Fettweis et al., 2006; Schartau et al., 2019). The POM content (measured as Loss-on-Ignition, LoI) of the SPM (not shown) varies between about 10% to more than 90%. The fraction of POC incorporated in SPM varies between ~2.5% and 30% (POC), while the PON fraction is clearly lower, ranging between ~0.35% and 4%. Thus, the POC and PON content of SPM are about 4 and 28 times smaller than the POM content respectively. From about a 100 mg/l SPM concentration onward the POC and PON content reach an asymptotic value of about 2.5% and 0.35% respectively. The 10 to 15 time increase of the POC and PON content occurs over two orders of magnitude in SPM concentration and shows that SPM in the nearshore contains proportionally significantly less OM than in the offshore (see Tables A.1 - A.3 in Appendix A for exact values). The best estimates of K_{POM}, f_1 and f_2 for annual (all year) representations of POC:SPM, PON:SPM and TEP:SPM are listed in Table 1. In all cases m_{POM} was taken as the best estimate for the POM model (eq. 4) for the LoI data set from the German Bight and amounts to 0.13 (see Schartau et al., 2019).

TEPs incorporate mainly organic carbon. Thus, measured TEP concentrations are not independent of the POC measurements, which is reflected in the significant ($p<0.05$) correlation between POC and TEP in the data with an $R^2=0.59$. Accordingly, the dependency between TEP and SPM concentration (Figure 5c) is similar to those found for POC and PON (Figures 5a and 5b). Instead of a percentage fraction of SPM, the TEP:SPM ratio is given here in mass units (g XG eq.)/g (Figure 5c), because the concentration of the Alcian blue stained microgels cannot be easily related to a mass concentration e.g. of organic carbon, in the presence of resuspended mineral particles. A derivation of a dependency between Alcian blue stained particles and their carbon content at different SPM concentrations is a relevant side aspect of our study (see Appendix D). The TEP:SPM ratio is approximately 0.05 (g XG eq.)/g at SPM concentrations

greater than 100 mg/l. With decreasing SPM concentrations, the ratio increases by one order of magnitude, to ~0.3 (g XG eq.)/g at SPM concentrations below 6 mg/l.

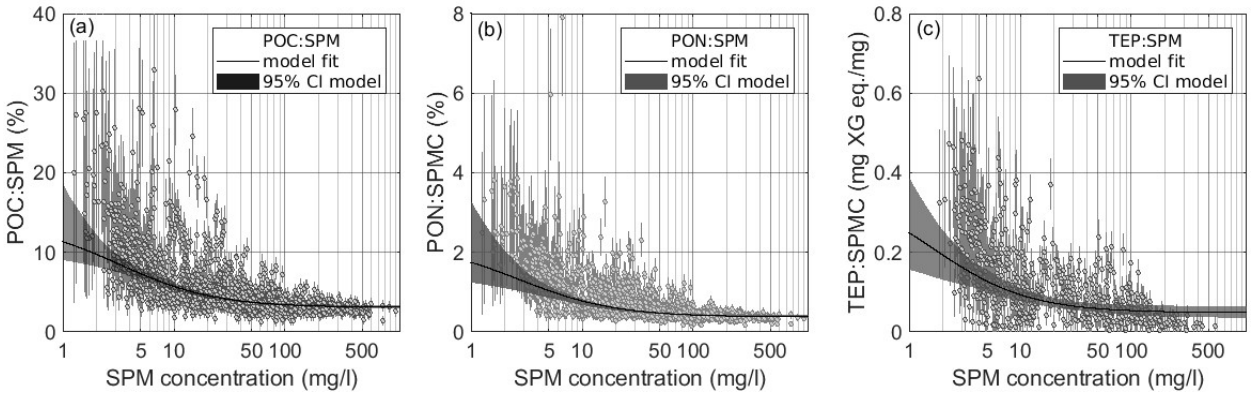

Figure 5: Model fit and 95% confidence intervals through all data for the POC content (left), PON content (middle) and the TEP content (right) as a function of the SPM concentration. The error bars represent the uncertainties of the measurements (see § 2.2.1). The shaded area is the 95% confidence interval of an ensemble of individual model fits, based on 100 optimizations with different, randomly sampled, data subsets.

3.4 Model Estimates of the Seasonally Sorted Data of POC, PON and TEP

The annual composite data of POC:SPM, PON:SPM and TEP:SPM, as depicted in Figure 5, exhibit extensive variability. For the most part, this variability can be attributed to seasonal changes. The fits of the models to annual composite data resolve and explain only differences between the different observational types. Seasonal variations have been further resolved by fitting the models to seasonally sorted data. Table 1 includes estimates of K_{POM}, f_1 and f_2 all four seasons separately. A higher resolution of temporal changes of parameter values was derived for model fits to TEP:SPM data, with monthly parameter estimates (see Table B.1 in Appendix B). In general, the non-linear dependency of the POC and PON content of SPM (Figure 6) varies in a similar way as the TEP:SPM ratio (Figure 7), with clearly altered seasonal signals.

At high SPM concentrations, greater than 100 mg/l, the variability remains small and temporal differences between the model solutions are indistinguishable for POC:SPM and PON:SPM. A large spread in the seasonally resolved model solutions were obtained for TEP:SPM ratio at SPM > 100 mg/l (Figure 7). The only noticeable difference is the lower estimate of f_2 obtained for modelling the TEP:SPM ratio at high SPM concentrations in winter. Whether this estimate is actually associated with a clear difference in the mineral-associated fraction of TEP in winter is unclear. Apart from this, the overall spread does not follow any seasonal pattern and must be attributed to larger uncertainties in the model fits of the TEP:SPM ratio. Overall, seasonal variations in the mineral-associated fractions of POC, PON, and TEP in SPM could not be identified and appear to be negligible. The small changes may rather be associated with variations in sediment types that contain variable constituents and fractions of minerals.

561 **Table 1**: Model parameters for POC, PON and TEP for all data (year) and for the four seasons.
562 The units for K_{POM} are mg/l (same unit as SPM concentration) and for f_1 and f_2 [g/(g POM)] for
563 POC and PON and in [g XG eq./(g POM)] for TEP.

m_{POM}=0.13	K_{POM} CI 95% [lower, upper]	f_1 CI 95% [lower, upper]	f_2 CI 95% [lower, upper]
Year			
POC	3.25 [0.24, 5.53]	0.122 [0.065, 0.981]	0.268 [0.248, 0.291]
PON	2.73 [0.13, 5.75]	0.021 [0.006, 0.203]	0.033 [0.031, 0.036]
TEP	1.61 [0.20, 4.36]	0.367 [0.100, 1.200]	0.422 [0.285, 0.583]
Winter			
POC	3.02 [1.34, 4.49]	0.058 [0.038, 0.112]	0.260 [0.248, 0.273]
PON	3.20 [2.16, 4.22]	0.008 [0.007, 0.011]	0.032 [0.030, 0.033]
TEP	4.25 [2.68, 6.00]	0.097 [0.058, 0.152]	0.251 [0.185, 0.318]
Spring			
POC	4.92 [3.11, 6.70]	0.197 [0.158, 0.261]	0.239 [0.216, 0.258]
PON	4.31 [2.95, 5.61]	0.032 [0.027, 0.038]	0.031 [0.028, 0.034]
TEP	3.67 [2.12, 4.83]	0.489 [0.386, 0.641]	0.457 [0.265, 0.677]
Summer			
POC	2.79 [0.28, 5.40]	0.173 [0.105, 0.993]	0.267 [0.237, 0.306]
PON	2.82 [1.34, 4.05]	0.028 [0.022, 0.043]	0.034 [0.031, 0.039]
TEP	3.27 [1.63, 4.62]	0.379 [0.281, 0.567]	0.456 [0.296, 0.601]
Autumn			
POC	2.18 [0.63, 3.62]	0.141 [0.085, 0.350]	0.282 [0255, 0.304]
PON	0.90 [0.08, 8.00]	0.033 [0.009, 0.106]	0.031 [0028, 0.033]
TEP	1.46 [0.10, 10.00]	0.267 [0.020, 1.200]	0.514 [0.392, 0.647]

564

565 For SPM concentrations below ~100 mg/l, we identified clear and distinctive seasonal
566 patterns. Our results show a correlation with season (and thus with primary production), which is
567 most pronounced in the low-turbid data. In all cases, the seasonal changes could be well resolved
568 (Figures 6 and 7). During the winter season the variations of the SPM's content of POC, PON,
569 and TEP remain small for a large range of SPM concentrations, with only a small increase of
570 respective fractions at low SPM concentrations. The general picture changes drastically for the
571 spring period when phytoplankton blooms induce a substantial increase in the POC and PON
572 content of the SPM, and also the TEP:SPM ratios follow this signal. At SPM concentrations of 1
573 mg/l, the lower end of the sample values, the POC and PON fractions of SPM are ~17% and
574 ~2.5%, and for TEP ~0.4 (g XG eq.)/g. During spring the measured POC and PON contents of
575 the SPM feature some high values at SPM concentration between 10 to 50 mg/l, which are not
576 captured by the model solution and are likely caused by the high spatio-temporal variability of
577 patches with elevated phytoplankton biomass concentrations. Still, the model's optimized
578 solutions for spring yield highest in the production of fresh POC, PON, and TEP in this range of
579 SPM concentrations. According to the optimized model solutions, the elevated spring values
580 gradually decrease during summer and autumn, a trend that can hardly be recognized on the basis
581 of the highly scattered sample data alone. The differences between the summer and autumn
582 signals are somewhat less distinctive than their differences to spring conditions. This is because
583 transitional months like September may include a prolonged bloom signal from summer or

involve secondary bloom events due to the recurrence of elevated nutrient concentrations. The transitions from autumn to winter conditions are again well pronounced.

The ratio $(f_{1,POC}):(f_{1,PON})$ = $(POC_f:POM_f)/(PON_f:POM_f)$ is indicative for the C:N ratio of the estimated fresh POM ($POC_f:PON_f$), while the same ratio for the f_2 parameter represents the C:N ratio of the estimated mineral-associated POM ($POC_m:PON_m$), see Table 2 and Figure C.1 in Appendix C. Both ratios have a seasonal variability, the $POC_f:PON_f$ ratio compares well with the POC:PON ratio from the observations, which confirms the credibility of our parameter estimates. The winter and autumn values of the fresh $POC_f:PON_f$ and of the $POC_{obs}:PON_{obs}$ are above the Redfield ratio (6.62 molN $molC^{-1}$) and the summer-spring values below it, but all values agree within the levels of uncertainty. The mineral-associated ratio $POC_m:PON_m$ is always above the Redfield ratio well beyond the lower 95% confidence limits (except summer), implying that the mineral-associated POM is more enriched in C than the fresh POM.

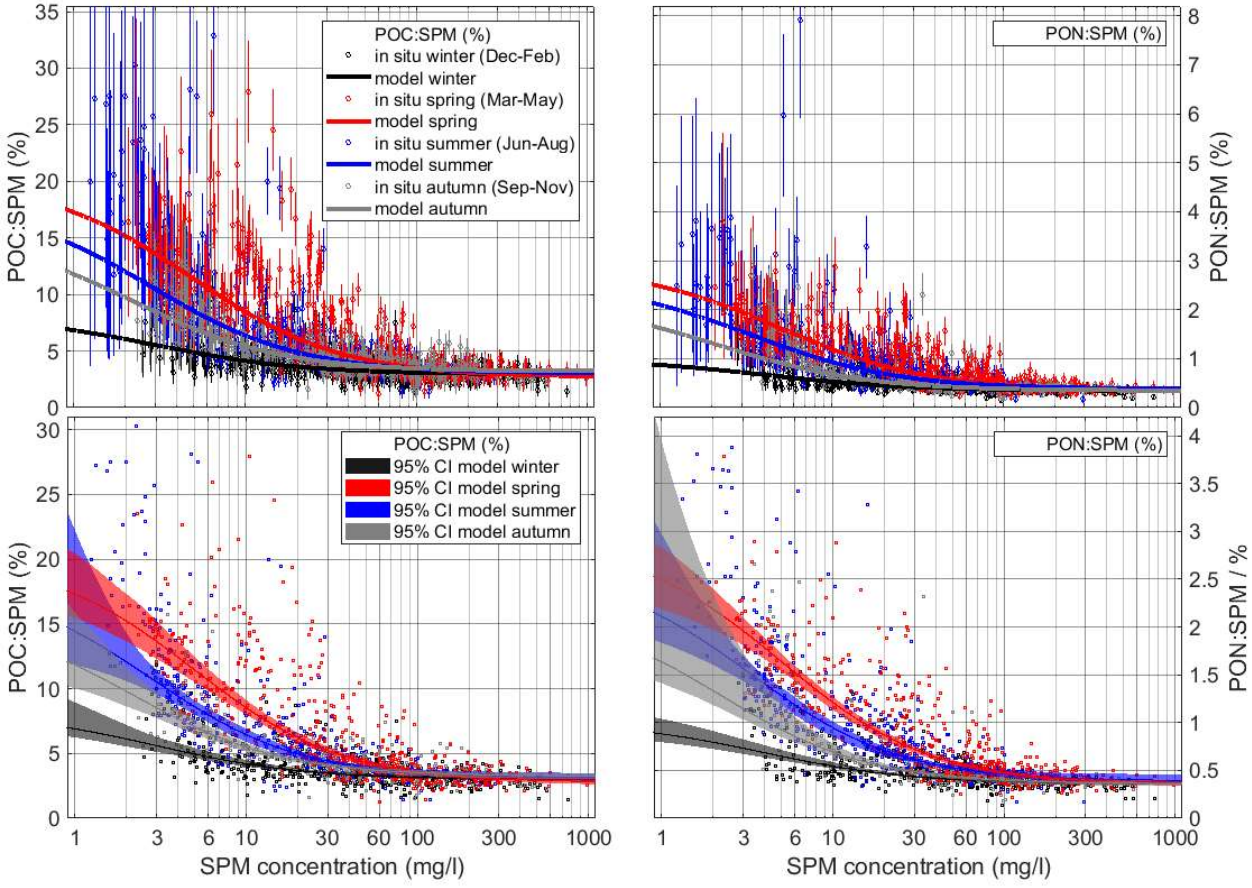

Figure 6: POC and PON content (in %) as a function of SPM concentration (data from 2004-2020). Top panels show the uncertainties of the data as described in § 2.2.1 and model estimates for the different seasons. Bottom panels show the 95% confidence interval of an ensemble of individual model fits, based on 100 optimizations with different, randomly sampled, data subsets.

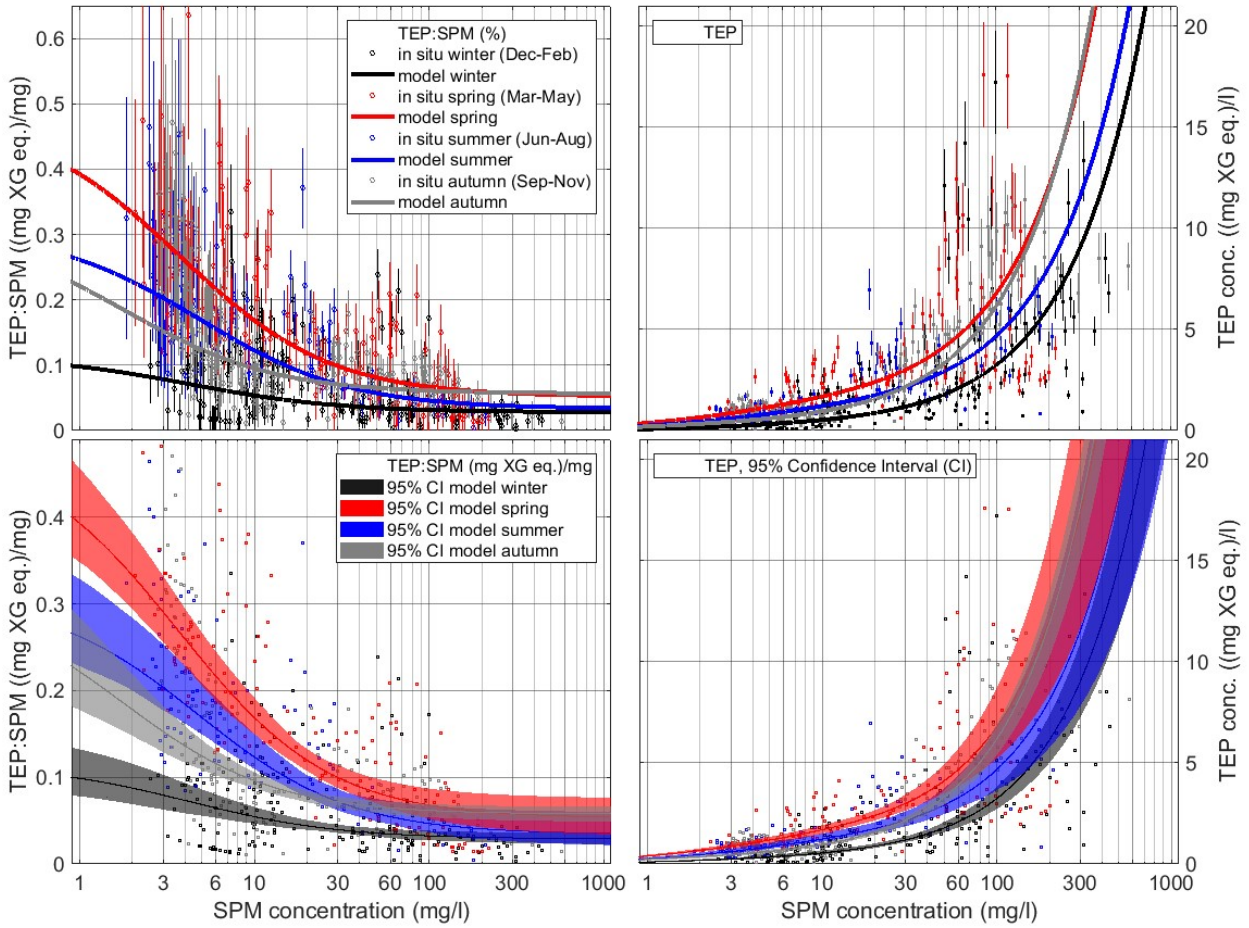

Figure 7: TEP content (left) and TEP concentration (right) as a function of SPM concentration. The lines are the result of the TEP-SPM model for the different seasons. The error bars represent the uncertainties of the TEP measurements, see § 2.2.1. Bottom panels show the 95% confidence interval of an ensemble of individual model fits, based on 100 optimizations with different, randomly sampled, data subsets.

Table 2: C/N ratios of the model parameters f_1(POC):f_1(PON) and f_2(POC):f_2(PON) and of the ratio POC_{obs}:PON_{obs} from in situ measurements.

	$f_{1,POC}$:$f_{1,PON}$ CI 95% [lower, upper]	$f_{2,POC}$:$f_{2,PON}$ CI 95% [lower, upper]	POC_{obs}:PON_{obs} CI 95% [lower, upper]
Winter	7.99 [4.35, 16.15]	8.39 [7.78, 8.98]	7.67 [5.27, 11.99]
Spring	6.85 [5.12, 9.14]	7.81 [6.80, 8.83]	7.13 [5.14, 10.19]
Summer	7.37 [1.41, >20]	8.06 [6.43, 9.95]	6.76 [4.99, 10.33]
Autumn	5.42 [2.66, >20]	9.12 [8.31, 9.96]	7.64 [5.11, 12.76]

4 Discussion

The main objective of the study is to investigate to what extent a model-based separation of the organic particulate matter into fresh and mineral-associated, i.e. fresh and labile versus more recalcitrant fractions, may unravel a signal that relates to the seasonal buildup and breakdown of flocs in coastal oceans. In principle, flocculation is depending on a number of local environmental conditions, e.g. turbulence, cation concentration, SPM concentration as a proxy particle number density, mineral composition, POM concentration and composition (e.g. TEP) and microorganism (Dyer, 1989; Mietta et al., 2009; Keyvani & Strom, 2014; Lai et al., 2018; Zhang et al., 2021). The bulk mineralogical composition of the SPM in the study area is relatively constant and consists of 32-39% clays, 25-33% carbonates, 12-18% quartz, 11-15% amorphous silicates and 5-8% feldspars and accessory minerals (Adriaens et al., 2019). The cation concentrations are high and well above the threshold for salinity induced flocculation so that flocculation in the study area is above all controlled by the POM composition of the SPM, the SPM concentration and the hydrodynamic conditions. The effect of turbulence and SPM concentration on flocculation in the study area has been described in previous studies (Fettweis et al., 2006; Fettweis et al., 2014; Fettweis & Baeye, 2015). They reported that maximum floc size was mainly controlled by turbulence intensity (tides and waves), which is higher in the nearshore area than offshore, but does not exhibit a pronounced seasonal signal. Our LISST data (Figure 3) confirm that the size of the largest flocs is similar during all seasons, but their abundance is higher in spring and summer, because they seem to be more tightly bound and resist better shear-induced breakup.

The seasonal dependence of SPM concentration with lowest values in summer (Figure 2d) contrasts with the inverse dependence of the median floc sizes which are highest in summer (Figure 4, left panel). Thus, SPM concentration in itself can be ruled out to explain flocculation and the qualitative properties of SPM may provide a much better clue. Given the large variability in SPM concentration within the nearshore areas and along their transition to the offshore waters, their variation may unravel predominant variations of the processes involved. In the following discussion we will show how the modified application of the POM-SPM model of Schartau et al. (2019) to the POC, PON and TEP sample data turned out to be beneficial. With the aid of the calibrated model solutions we could estimate how the relative fractions of freshly produced labile and semi-labile OM (of POC, PON, and TEP) along with the rather recalcitrant mineral-associated OM content of the SPM change with SPM concentration. A starting point of this approach is the obvious concurrence of seasonal rises and declines in median floc size (Figures 3 and 4) with the model parameter K_{POM} , which numerates the seasonal built up of fresh organic material and its components (Figures 5-7 and Table 1). Our synthesis between model application and in situ measurements delivers important insight into the complex process of flocculation in a region of great variability. Based on results of our analyses we can expand the scope of discussion on how the fresh and the mineral-associated OM fractions of the SPM affect the process of biophysical flocculation.

4.1 Spatio-Temporal Variations of Floc Characteristics

Flocs in the nearshore high turbid station MOW1 were subject to extensive temporal variations in volume concentration, density and size during a tidal cycle (Figures 2 and 3). The FSDs were skewed towards smaller sizes around peak flow (blue in Figure 3) and developed a peak in the larger size classes around slack water (red in Figure 3). Lee et al. (2012) have shown

that the flocs at MOW1 are characterized by a multimodal size distribution that consists of small particles, flocculi, microflocs, and macroflocs. The smallest particles likely consist of clay-sized particles of various mineral composition, the flocculi are breakage-resistant aggregates of clay minerals, microflocs can be attributed to the medium size aggregates, whereas macroflocs can be identified as the large aggregates with diameters up to a few hundred micrometers. Tran and Strom (2017) have shown in a laboratory experiment that silt and clay combine into flocs. In some contrast to this, we observe (Figure 3 and 4) that the FSDs at MOW1 all had well pronounced modes within the smallest size classes in winter. This mode diminished towards summer. This indicates that in winter abundant fine-grained mineral particles do not aggregate into flocs. They settle slowly and remain in suspension longer, resulting in a background turbidity that is higher than in summer. In general, lower turbulence intensities before slack water promote the aggregation of the more mineral (i.e. with a POC content of about 3%) flocculi and microflocs into larger macroflocs. In winter these macroflocs have similar characteristics than the microflocs, i.e. they are mineral enriched (Tang & Maggi, 2016). In summer, according to Fettweis and Baeye (2015), the small particles, flocculi and microflocs also coagulate with freshly produced OM to form quite stable aggregates that are enriched with biogenic substances, including phytoplankton cells and detrital substances. These spring and summer flocs have lower densities than the winter and autumn flocs (see Figure 2g and Tables in Appendix A) but reach floc sizes that involve settling velocities that exceed those of the smaller winter flocs leading to their accumulation near the bed and the decrease of the average SPM concentrations in the water column.

In contrast, in the offshore stations W05 and W08, the seasonal variabilities in the concentration of SPM and the OM parameters were less pronounced and the FSD distribution rather constant over the tides (Figure 3), showing that here aggregation dominates disaggregation kinetics (Fettweis and Lee, 2017). The principal variations in these parameters occurred between seasons and not within tides. In winter and autumn, the FSDs were multimodal, with a first mode around 10 µm, a second one around 50-100 µm and a third one around 300 µm (Figure 3). The first mode could consist of flocculi, while the second mode could be formed by minerals from biogenic origin (carbonates, amorphous quartz). In spring, the 300 µm peak dominated the FSDs. In summer, the increase of the median floc size in these offshore stations (see Figure 2) indicates that the observed decrease of the lower modes is caused by the incorporation of these particles into the larger aggregates. These larger biological aggregates can be lighter and even settle slower than smaller bio-mineral aggregates found at MOW1 (Maggi & Tang, 2015).

4.2. TEP Concentration and its Relation to Floc Size

4.2.1 Seasonal Variation in TEP Concentration

A correlation of TEP concentrations with the rise and decline of phytoplankton blooms is reported from lab cultures (Fukao et al., 2010), estuarine and nearshore areas (Ramaiah et al., 2001; Bhaskar and Bhosle, 2006; Chowdhury et al., 2016), and from the open ocean (Mari et al. 2017). Others report temporary disconnection of TEP from Chl-a concentrations (Ortega-Retuarta et al., 2017, Lee et al., 2020). Our data do not show a close relationship between Chl-a and TEP concentration (See Figure 2j and 2l). In the shallow nearshore station MOW1 a substantial fraction of TEP seems to be rather mineral-associated, entering the water column via resuspension of sediment particles. The TEP concentration followed the SPM concentration irrespective of the season and thus also during winter when primary production has largely

ceased (Figure 2d, 2j and Figure 7, right panel). This general dependency is modulated by a seasonal signal, depending on the amount of POC and PON being built up via primary production. Our seasonal pattern is in line with findings from the turbidity maximum of the Seine estuary (Morelle et al., 2018). There, the highest TEP concentrations coincide with the lowest EPS and DOC concentration in winter and vice versa in summer. In contrast, the more offshore stations, where SPM concentration remained most of the time below 10 mg/l, had TEP and POC concentrations that were generally higher in spring and summer than in winter. The offshore environments with low turbid conditions agree with the correlation found by Mari and Burd (1998) between DOC and TEP concentrations suggesting that TEP are formed by coagulation of the dissolved EPS (Mari & Burd, 1998). These results indicate the occurrence of two types of TEP, presumably having different chemical characteristics with respect to their stickiness and their potential to promote the formation of flocs of large size.

An immediate dependency between the total abundance of TEP and floc size cannot be inferred from our data. The interpretation of the results for the station MOW1 is complicated by the fact that similar TEP concentrations resulted in different floc sizes in winter and summer (see Figure 2f and 2j). Morelle et al. (2018) have explained the higher TEP concentration in winter by deposition and resuspension processes. This would mean that due to the larger flocs in spring and summer, a large part of the TEP is found in the benthic boundary layer or on the bed, while in winter it is resuspended. However, this interpretation does not explain why floc sizes were smaller in winter and is not supported by studies relating floc size to TEP concentration (e.g. Passow, 2002; Verney et al., 2009; Deng et al., 2019) and by our data that show larger floc sizes in spring and summer. Our analysis suggests that biophysical flocculation in highly turbid areas is strongly affected by the occurrence of fresh OM rather than the total amount of OM. TEP production rapidly increased when the maximum capacity for the build-up of fresh POC and PON was reached (Figure 8). This occurs when phytoplankton approaches nutrient limited growth conditions (Engel et al., 2004; Schartau et al., 2007). Part of the fresh OM consists of EPS and will partly be transformed into TEP. We could not explicitly resolve the process of TEP formation from dissolved precursors, but found generally higher DOC concentration in spring and summer. Figure 2k shows that DOC concentration, which contains EPS, has a maximum in late spring and summer, as in the Seine estuary (Morelle et al., 2018).

In order to assess the relationship between the time evolution of SPM and TEP in their quantities and qualities, Figure 9 shows the low-pass filtered median floc size data at the high turbid station MOW1 (as in Figure 4) together with the low-pass filtered long-term SPM concentration time series (upper panel), as well as the seasonal evolution of fresh and total TEP concentration (lower panel) derived from calibrated results of the TEP-SPM model based on monthly model parameter estimates of K_{POM}, f_1 and f_2 (Appendix B). When fresh TEP is produced (from half February onward), the median floc size increases (in particular from March on, when the proportion of fresh TEP to total TEP ratio increases) and SPM concentration decreases. Although fresh TEP concentration is at its maximum in early spring, the increase in median floc size, the changes in floc size distribution (Figure 4) and the decrease in SPM concentration occur more gradually. The progressive raise in floc size follows the increase and the decrease of the fresh TEP fraction (TEP_{fresh}:TEP_{total}). This ratio is low during winter (about 2%) and starts to increase from the beginning of February to about 15% in March and then more quickly to reach a maximum around 60% in May-June. The peaks in floc sizes as well as the lowest SPM concentrations were observed during this period.

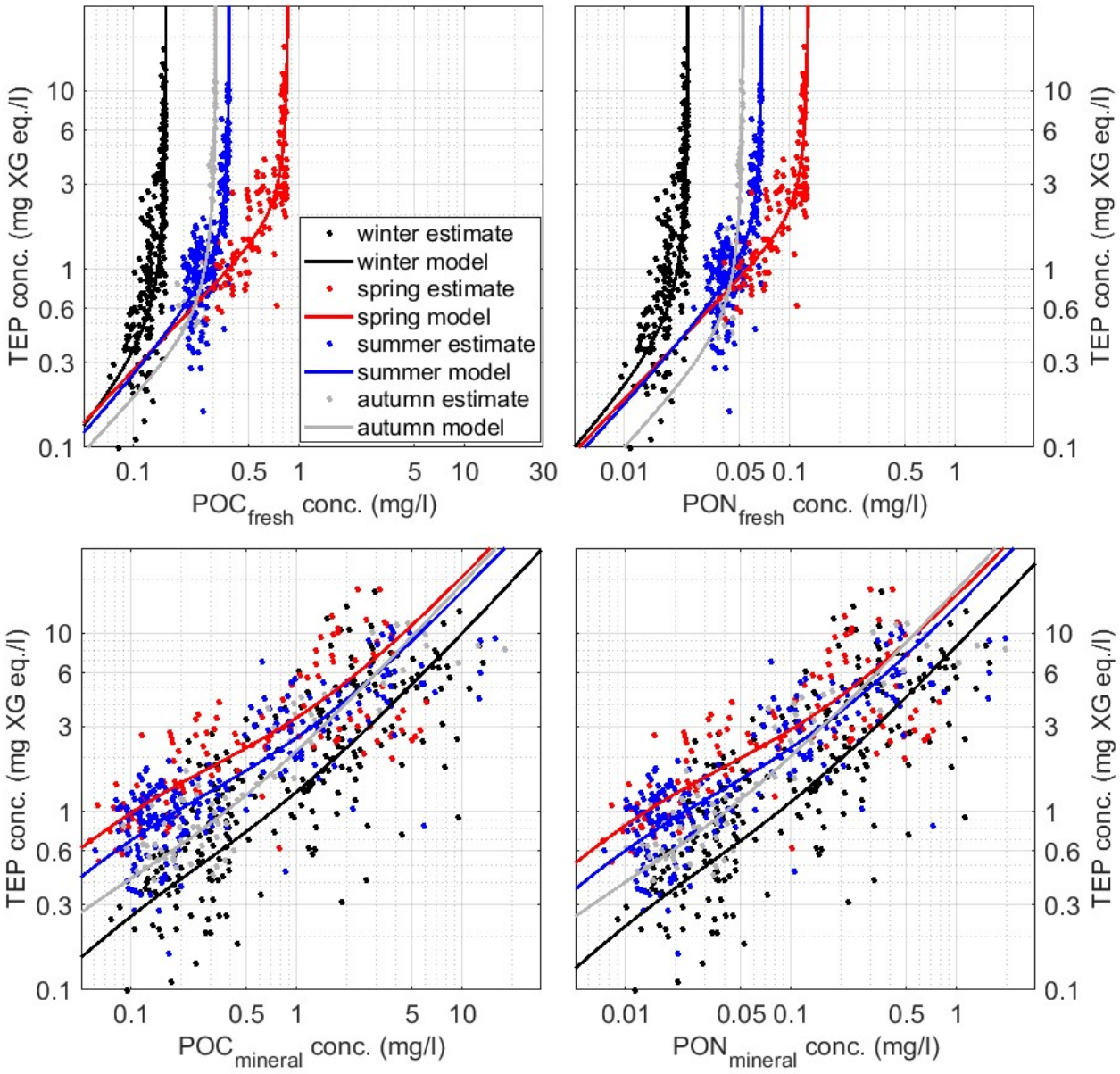

745

746 **Figure 8**: The observed total TEP concentration versus the model derived fresh (upper panel)
747 and mineral-associated (lower panel) POC and PON concentration. The lines are the estimated
748 total TEP concentration as a function of POC and PON concentration derived from the POM-
749 SPM model.

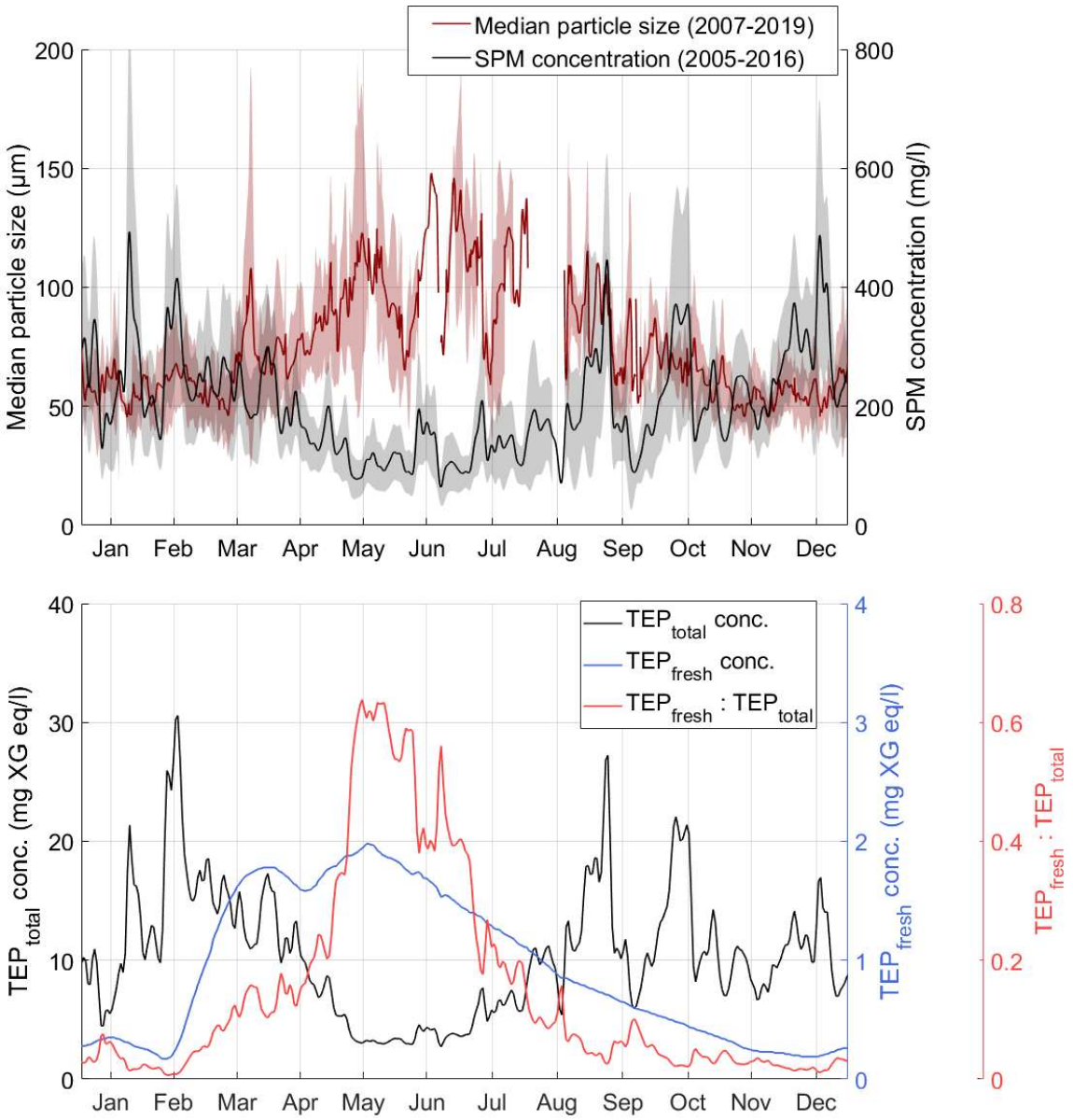

Figure 9: (a) Long-term and low-pass SPM concentration (2005-2016) and median floc size (2007-2019) at 2 m above bed. The shaded area is the standard deviation if more than 2 data points are available. (b) The model estimates of total (black) and fresh (blue) TEP concentration calculated from the long-term SPM concentration time series. The red line is the fraction of fresh TEP in the total TEP. All data are from the near shore station MOW1.

The decrease of the fresh TEP concentration after its quick accumulation in spring occurs gradually over a period of about 6 months (May-November) and can be due to hydrolyzation, consumption and/or deposition. This is in contrast with the early spring period, where most of the fresh TEP accumulation occurs within about one month (February-March), before reaching a maximum in early May. The production of fresh TEP correlates with the first increase in Chl a concentration in February in 2019 and the first decrease of SPM concentration from beginning of March onward (Figure 10). These findings support the hypothesis that in early spring in the turbid nearshore, when light conditions are still depleted, light adapted phytoplankton species

initiate the spring bloom and also induce the formation of fresh TEP. In contrast to the mineral-associated TEP, it is this initial occurrence of fresh TEP that eventually promotes aggregation and the formation of larger flocs with higher settling rates. This in turn lowers SPM concentration and reduces light attenuation, which paves the way for species with higher light requirements in the phytoplankton seasonal succession. Altogether, the results underline that the different components of the SPM (i.e., mineral, organic matter and living particles) form an integrated dynamic system with direct interactions and feedback controls.

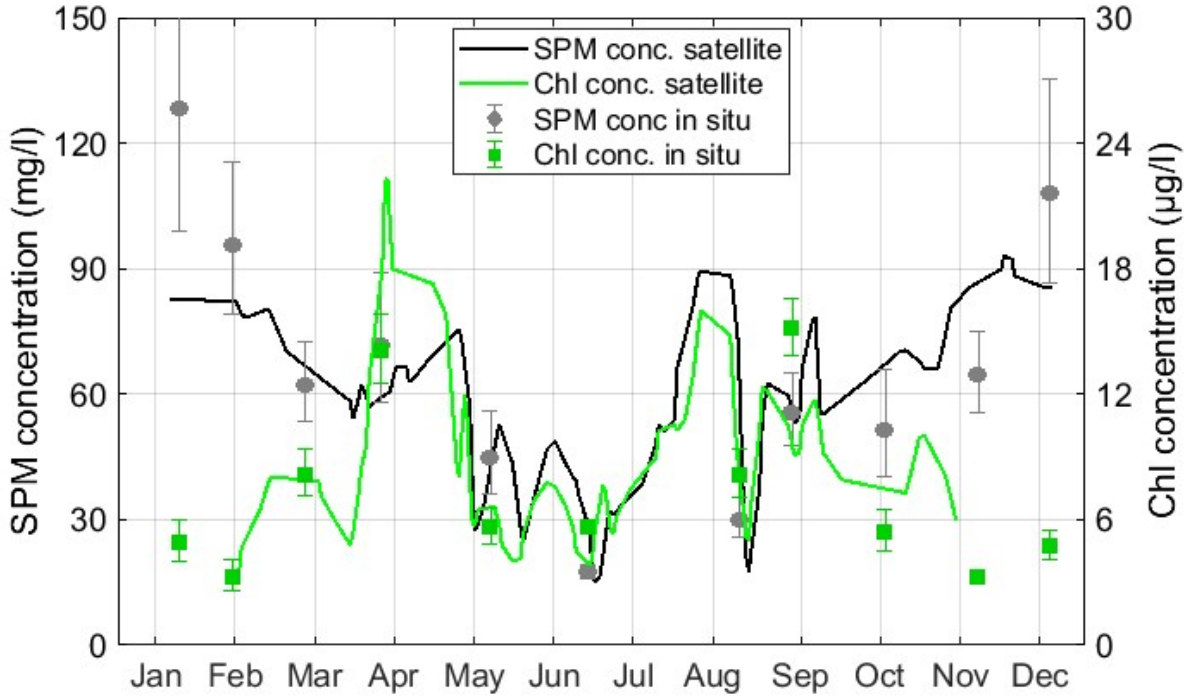

Figure 10: Time series of surface SPM and Chl-a concentration in 2019 derived from remote sensing (Sentinel-3/OLCI) and in situ observations at station MOW1 (nearshore). The in-situ data are mean values over a tidal cycle, the error bars are the standard error of the mean.

4.2.2. TEP in Autumn and Winter

What are the quantitative and qualitative characteristics of TEP outside the growth season? The presence of high concentrations of TEP in autumn and winter above all in the turbid nearshore (Figure 2k) raises questions on the characteristics of this organic matter. Mari et al. (2007) mention that the efficiency of the transformation of EPS into TEP and the TEP reactivity decrease with time. This would mean that the TEP stickiness varies as a function of the degradation stage and age. Winter TEP would then be smaller in size and less sticky, while in spring and summer it would consist of larger and more sticky particles that become actively involved in flocculation dynamics (Engel et al., 2020). The biomineral flocs resist better to shear-induced break-up in spring and summer due to availability of more reactive TEP and of the inclusion of free-floating bacteria and other microorganisms into the flocs that produces themselves exopolymers (Fettweis et al., 2014; Jachlewski et al., 2015; Shen et al., 2019). The bacteria associated with TEP contribute to the hydrolysis of the OM and thus foster the gradual decay and disaggregation of the biomineral flocs in autumn (Smith et al., 1992; Alldredge et al., 1993; Passow & Alldredge, 1994), which is reflected in the observed decrease in floc size in our

data. As the transition from summer to winter is gradual, one would expect that TEP concentration decreases through microbial respiration until a minimum is reached just before the onset of the algae bloom in early spring. The latter is observed in the low turbid offshore stations W05 and W08, but not in the turbid MOW1 station, see Figure 2j. Other studies highlight the relationship between OM content and mineral surface area (Keil et al., 1994; Mayer, 1994). This means that with increasing SPM concentration, the OM concentration and thus also TEP concentration increases, while the POM content of the SPM decreases until reaching an asymptotic value at high SPM concentrations (>100 mg/l) of about 3% POC, 0.4% PON, and 0.04 (mg XG eq.)/mg TEP (Figures 5-7). At high SPM concentrations the fresh OM represents only a small part of the total OM and is hardly detectable due to the high variability of the measurements. Both the fresh and recalcitrant OM can be associated to the mineral surfaces, being protected from microbial respiration (Keil et al., 1994; Kalbitz et al., 2005; Hemingway et al., 2019; Chen et al., 2021). The protected mineral-associated OM explains the high TEP concentrations in winter in high turbid areas such as the Belgian nearshore, Chesapeake Bay (Malpezzi et al., 2013) or the Seine estuary (Morelle et al., 2018).

The mineral-associated POC over TEP ratio is about 1 in winter and between 0.52 and 0.59 (mean 0.56) during the other seasons (see Appendix D). The higher ratio in winter is the result of the optimal estimation of the POC and TEP content in the SPM based on our data. The model estimates a lower value of the TEP content in the SPM in winter at high SPM concentrations than for the other seasons (Figure 6). Such distinction could be explained by a lower amount of mineral-associated TEP in winter and by the occurrence of two different mineral-associated TEP fractions. One is more recalcitrant and remains, while the other one is still subject to gradual but slow degradation and eventually disappears in winter. The first one could consist of the TEP that occurs in between the layers of the clay crystal structures (Mayer, 1994; Blattmann et al., 2019). The second one could consist of a semi-labile biofilm on the surface of the mineral particles (Decho & Gutierrez, 2017). Anyway, the mineral-associated POC over TEP ratios indicates that the recalcitrant mineral-associated TEP makes up a great portion of the mineral-associated POC.

To conclude, while also present during autumn and winter, fresh TEP occurs at much lower concentration then. It could originate from winter biological activity, from bacteria or phytoplankton (Chl-a concentration in winter is on average between 1.1 µg/l at W08 and 3.5 µg/l at MOW1, see appendix A). The flocs in autumn and winter can thus be considered as biophysical in nature as few fresh TEP is available to aggregate cohesive particles (such as clay minerals) with non-cohesive ones (such as carbonates) into larger floc. The rising tails in the winter FSD at MOW1 (Figures 3 and 4) point to the occurrence of particles smaller than the measuring range of the LISST (i.e. 2.72 µm) and indicate that the efficiency of biophysical aggregation in winter is, however, much lower than in spring and summer in the high turbid nearshore.

4.3 Spatial Variation in SPM Composition

4.3.1 Asymptotic Decrease of OM Content with Increasing SPM Concentration

The surface sediments at W05 and W08 consist of medium sand with small amounts of fines (a few %) and POC contents in the fraction <63 µm of about 1.8% and 1.1% respectively. These values are lower by a factor of 4 and 8, respectively, than the mean POC content of the

SPM in these stations (see Tables A.2 and A.3 in appendix A). In these stations the SPM concentration was generally below 10 mg/l. This is a clear indication that the suspended material can only to a minor part originate from the sea bed. This illustrates nicely the increasing decoupling of near bed and water column processes with water depth and distance from the coastline. In the nearshore station MOW1, the amount of the fraction <63 µm in the sediments is about 50% (Fettweis and Van den Eynde, 2003), the POC content of the surface sediments (fraction <63 µm) is only lower by a factor of 1.5 than of the SPM at high concentrations (2% versus 3%) and indicates that the surface layer of the seabed is actively involved in the tidally induced resuspension and deposition of the particulate material (Table A.1 in appendix A). The asymptotic value of 3% POC at high SPM concentration shows that the minerals are saturated and that no long-term accumulation of OM occurs in the nearshore station MOW1. The fresh OM that is not associated with the mineral surfaces will thus quickly be consumed in the food web. Similar values of the POC contents of the SPM have been found in the turbidity maxima of the Seine and Loire estuary (Etcheber et al., 2007), lower ones in the Gironde estuary (Etcheber et al., 2007) and higher ones in the Yangtze (Milliman et al., 1984) and Congo river (Bouillon et al., 2012). It is remarkable that these variations in POC content between different areas are relatively small (2%-5%), which points to a similar composition of the SPM in many turbid aquatic ecosystems over the world. The small differences are probably caused by methodological differences, measuring uncertainties and by different mineral-associations of the SPM, as the preservation of OM is controlled mainly by its clay mineralogy (Blattmann et al., 2019).

4.3.2 Nearshore to Offshore Gradient in Fresh and Mineral-Associated OM

We used the Sentinel-3/OLCI satellite images of SPM concentration to extract the cross-shore variation of mineral-associated and fresh components of POM, POC, PON and TEP at the water surface. Taking the model parameters for f_1, f_2, K_{POM} and m_{POM} (see Table 1), we applied the model pixelwise to the remote sensing data. In this way we generated eight further secondary satellite products purely based on SPM surface concentration. For the purpose of this study we discuss these data for all seasons along a transect the connects the three measuring stations from the coast (MOW1) with SPM concentration ≅80 mg/l via W05 to the offshore (W08) with ≅2 mg/l (see Figure 11).

The mineral-associated part (middle) follows to a large part the SPM concentration and has the same strong decrease with increasing distance from the coast. The fresh POM (left) in contrast, nearly keeps his level along the whole transect. The major seasonal formation of fresh POM thus occurs not only within the shallow coastal regions but extends along the whole area. These patterns are similar for all components of the POM and TEP and for all seasons. For the mineral-associated parts, winter has the highest and summer the lowest values except for TEP where the highest values are during the periods of spring and autumn blooms. The fresh parts are always highest in spring and lowest in winter. The ratios of fresh to mineral-associated POC, PON and TEP (right) show that there is a zone somewhere around station W05, where both fractions are about equal (ratio = 1). This may be identified as a transition zone where, seen from the land, the near coast conditions with particle dominance from the sea bed turn into open sea conditions with particles who are of pelagic origin. This transition zone is located in between MOW1 and W05 in spring and summer at a water depth around 10 to 15 m and corresponds with a surface SPM concentration of about 40 mg/l in spring and about 20 mg/l in summer. It is located more offshore in autumn where it occurs around W05 (water depth around 20 m) with about 8 mg/l SPM concentration and close to W08 in winter.

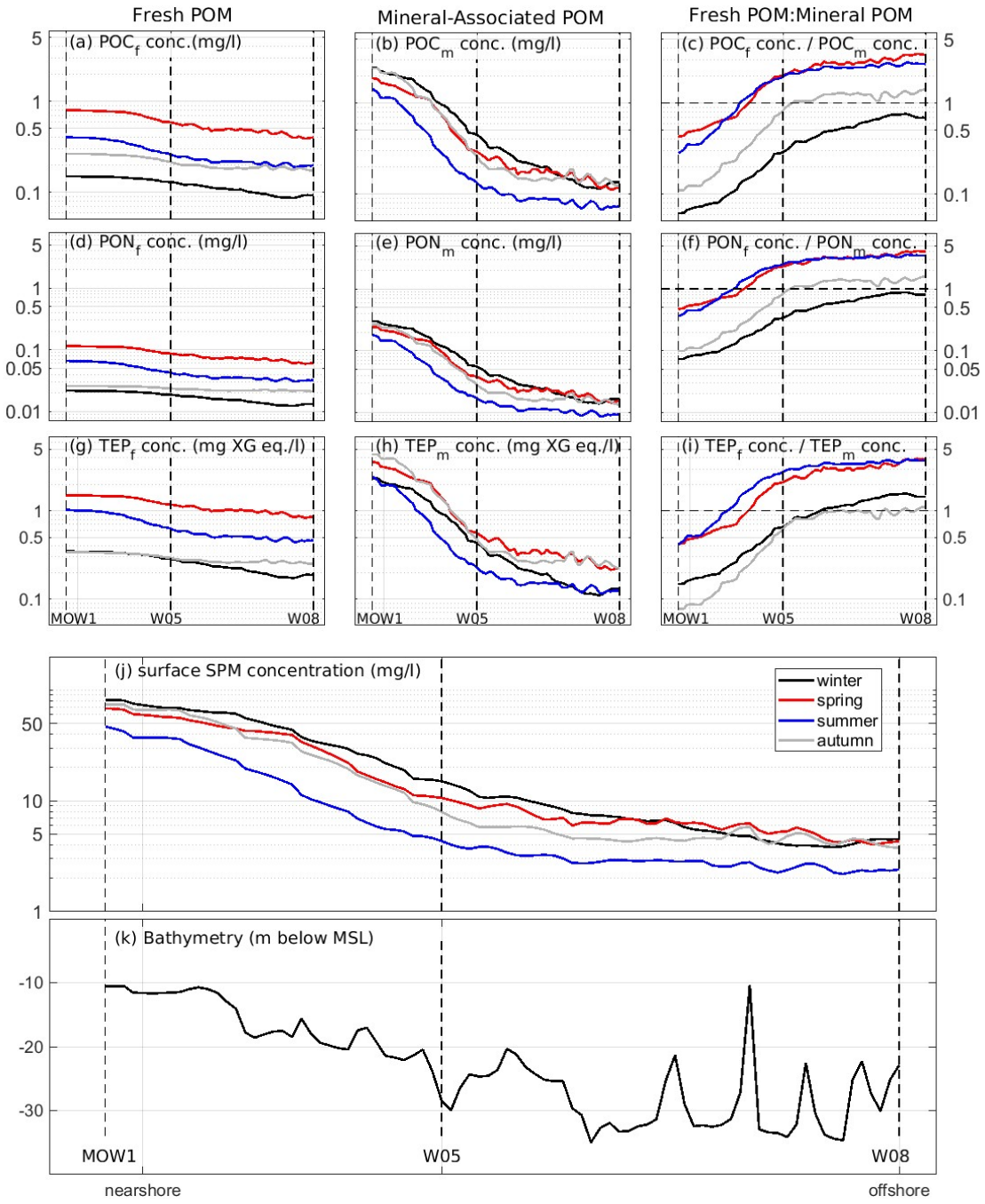

Figure 11: Model estimates of the nearshore (MOW1) to offshore (W08) fresh (left column) and mineral-associated (middle column) POC (a-b), PON (d-e) and TEP (g-h) concentrations calculated from the Sentinel-3/OLC derived surface SPM concentrations (j) using the model parameters of Table 1. The right column shows the ratios of fresh to mineral POC (c), PON (f) and TEP (i) concentration. Values above 1 have a fresh POC, PON or TEP concentration that exceed the mineral-associated one. The lower panel (k) shows the bathymetry (m below mean sea level) along the transect. The large changes in bathymetry between W05 and W08 are from sandbanks.

4.4 Consequences for the Modelling and Monitoring of Coastal Ecosystems

Changes in coastal ecosystems are often correlated with changes in water clarity or SPM concentration and thus with the POM content of the SPM (e.g. May et al., 2003; Capuzzo et al., 2015). The composition of SPM is the result of multiple natural processes that reflect the continuous mixing of marine and terrestrial particles of various ages and origins over geological time scales (Adriaens et al., 2018). Also, human activities have impacted the SPM concentration and composition. While the strongest anthropogenic changes in the study area occurred during the last decades, human occupation and landscape development date back to the last two millennia. They inevitably have had an impact on SPM composition and concentration (Baeteman et al., 2002). In the last decades, the North Sea has been subject to changes in SPM concentration and biological activities amongst which are the decrease in phytoplankton production and changes in community structures (Capuzzo et al., 2018; Nohe et al., 2020); the shift in chlorophyll a phenology (Desmit et al., 2020); the imbalance in the biogeochemical cycles of nutrients (Rousseau et al., 2006, Desmit et al., 2018); and the increase of the SPM concentration due to major construction works (Van Maren et al., 2015).

The area where the concentration of fresh and mineral-associated POM is about equal is of particular interest Schartau et al., 2019). For the German Bight, this transition zone is typically found at water depths of approximately 15 to 20 m along cross-shore transects and is characterized by a maximum of the settling velocities (Maerz et al., 2016). Human activities, e.g. dredging and dumping operations in the turbid nearshore, wind farms in the low turbid offshore areas or the effect of global warming (Fettweis et al., 2012; Jaiser et al., 2012; Baeye et al., 2015; Høyer & Karagali, 2016) might influence the localization of this transition zone and could make it a key element in monitoring programs such as the EU Marine Strategy Framework Directive. With our data-model syntheses we could consolidate a relationship that can be applied to SPM concentrations derived from other sources, e.g. from in situ long-term observations using optical and acoustic sensors or from remote sensing. A good example for such an application was documented by Schartau et al. (2019) for resolving spatio-temporal variations in fresh and mineral-associated fractions of POM in the German Bight. Though still imperfect, the application of the refined model to satellite SPM concentration products or high-resolution in-situ time series of calibrated optical or acoustical instruments will yield spatio-temporal compositional changes of the SPM, with respect to POC, PON, and TEP, both on large scales and for anomalous events. This greatly facilitates the monitoring of water quality parameters along the gradient from a domination of mineral-associated OM towards a domination of fresh OM, as documented in Figures 9 and 11, and enhances its information content without the increase of resources.

Many oceanographic quantities are often inaccessible to direct observation, due to the high cost of in situ sampling, the limitation of the standard water quality parameters and the low spatial and time resolution. Proxies, based on automated, highly resolving instruments are valuable as they help to extend undersampled or unobserved parameters. In this regard, SPM concentration as a proxy for POM, POC, PON, and TEP concentrations seems to be a key ingredient for the assessment and calibration of numerical models of coastal waters, ranging from SPM transport and deposition to key ecosystem processes.

Specifically, we have shown that the floc size distribution depends on the SPM concentration and on the availability of fresh TEP. In areas where the fresh over mineral-associated TEP is about unity and the SPM concentration low, flocculation occurs on a seasonal

time scale rather than a tidal one (Figure 3). In high turbid environments flocculation occurs on both a tidal and seasonal time scale (Figure 3, 4 and 9). Our model-based differentiation between fresh and mineral-associated POC, PON, and TEP shows, that SPM concentration can be used as a proxy of the flocculation kinetic model parameters (i.e., break-up and aggregation) adopted in numerical SPM transport models.

5 Conclusions

The relevant processes and the critical parameters that drive the mutual interactions between sediment and biological dynamics occur on a wide range of spatial and temporal scales. The OM content of the SPM is highly variable due to physical processes, such as tides and waves, varies with season due to biological activities and with the SPM concentration. There is a distinct difference between the offshore, more open ocean, and the turbid nearshore conditions. In the turbid nearshore areas where SPM concentration often exceeds 100 mg/l the OM fraction in association with the mineral particles is dominant, masking the smaller signal of fresh OM produced by primary production. In contrast, in the offshore stations the fresh OM components prevail and therefore explain most of the variability seen in the SPM concentration. POC and PON measurements represent bulk properties of the OM in suspension, combining compounds of various types from labile, semi-labile, to refractory OM as well as specific components such as TEPs and pigments. Our data demonstrate that biophysical flocculation cannot be explained by these bulk observables. However, a model-based separation between a more reactive labile and a less reactive mineral-associated fraction of POC, PON and specifically TEP is a productive approach to make the impact of OM on the flocculation process detectable under long-time field observations. From our data-model synthesis we learned that the median floc size increases only when fresh TEP becomes a substantial fraction of the SPM. With our study we could resolve the contradiction that similar TEP concentrations result in different floc sizes in winter and summer. Our results document that fresh TEP is one of the important controls of particles settling in coastal waters.

POM is associated with the mineral fraction and primarily with phyllosilicates (clays). It is therefore no surprise that the POM concentration increases with SPM concentration in coastal waters where due to water depths below 20 m and changing turbulence levels from tidal currents and waves, significant exchanges between pelagic and sea bed material exist. The fresh POM, and more specifically the presence of fresh TEP in spring and summer is not associated with these minerals but rather with the phytoplankton activity. This fresh TEP is responsible for the formation of larger biophysical flocs in spring and summer in the high turbid areas rather than the total TEP concentration. The nearly absence of fresh TEP in winter as a glue after particle collisions limits the floc sizes. Our results underline that the different components of the SPM, which are mineral, organic matter and living particles, form an integrated dynamic system with direct interactions and feedback controls.

Collecting data, such as SPM, POC, PON and TEP concentrations, from samples in the oceans or coastal seas, is expensive and often biased towards moderate weather conditions. Especially, anomalous, short-term events can often not be captured as shipping schedules are planned long in advance. SPM concentration, however, as a key proxy, can be measured either by remote sensing or automated in-situ systems. Samples then are only needed for better calibrations of these instruments. We have shown that these standard water quality measurements can be used to provide mathematical descriptions of additional complementary information, such as fresh and

mineral-associated POM. The models can be applied to measurements from optical or acoustical sensors or satellites to generate further secondary data products. Our approach could change the scope of in situ observations from merely the collection of data towards the improvement and validation of models that describe fundamental aspects of SPM composition in coastal seas. The availability of proxies could have important implications for future monitoring programs, as they may fill the lack of continuous long-term data of POM properties and as such could help to improve the efficiency of our monitoring systems by identifying more efficient locations for water sampling or for the deployment of observational instruments.

Authors contributions

The conceptual idea of the study had been developed by MF, XD, NT, MS and RR. MF, XD and NT conceived and designed the water sampling and analyzed the data together with RR. MF and BJL analyzed the LISST data from long-term and tidal cycle measurements. MF analyzed the long-term SPM sensor measurements. DvdZ analyzed the remote sensing data. MS devised the model and implemented the framework for parameter estimation. MS performed all model calibrations and worked out the associated statistical analyses. MF is lead author, who incorporated ideas, individual text contributions and revisions from all co-authors. All authors helped attaining overall coherence of this study.

Acknowledgements

The research was supported by the Belgian Science Policy (BELSPO) within the BRAIN-be program (BG-PART project), the Maritime Access Division of the Flemish Ministry of Mobility and Public Works (MOMO project), and the RBINS BGCMonit program. Scientific input from Markus Schartau and Rolf Riethmüller are integrated in the research programs "Marine and polar life" and "Coastal zones at a time of global change" funded by the Helmholtz Association of German Research Centers. Ship time with the RV Belgica was provided by BELSPO and RBINS–OD Nature. We thank L. Naudts and his team (RBINS-MSO) for all technical aspects of instrumentation and moorings and K. Parmentier and his team (RBINS-ECOCHEM) for the laboratory analysis of the samples.

The data (water samples, sensor measurements and remote sensing) used in this study can be found at url.

Appendix A: Tables with Mean Values

Table A.1: MOW1 (2004-2020), geometric mean and multiplicative standard deviation for the particulate and dissolved parameters (TDN: total dissolved nitrogen, TDP: total dissolved phosphate, Si: silicate) and arithmetic mean and standard deviation for the seabed parameters.

	year		winter		spring		summer		autumn	
	mean	std	mean	std	mean	std	mean	std	mean	std
Particulate parameters										
Hach Turbidity (FNU)	57	*2.39*	80	*2.28*	59	*2.20*	30	*2.42*	60	*2.17*
SPM-mass conc. (mg/l)	70	*2.32*	91	*2.25*	77	*2.41*	41	*2.14*	69	*2.09*
SPM-vol conc. (µl/l)	249	*3.32*	353	*2.45*	227	*3.25*	90	*2.33*	395	*3.48*
Median floc size (µm)	64	*1.89*	53	*1.73*	61	*2.00*	78	*1.82*	69	*1.89*
Effective floc density (mg/l)	246	*2.48*	370	*2.11*	228	*2.46*	117	*2.02*	320	*2.30*
POC conc. (mg/l)	2.62	*2.05*	2.91	*2.10*	3.20	*2.01*	1.61	*1.66*	2.56	*1.97*
PON conc. (mg/l)	0.35	*1.99*	0.38	*2.04*	0.44	*1.93*	0.23	*1.61*	0.33	*1.97*
TEP conc. (mg XG eq. /l)	3.57	*2.05*	2.80	*2.34*	4.12	*1.95*	3.30	*1.66*	4.61	*1.85*
Chl-a conc. (µg/l)	5.75	*2.50*	3.47	*1.94*	12.94	*1.93*	8.81	*1.66*	3.78	*2.46*
Pheo-a conc. (µg/l)	0.41	*2.36*	0.41	*2.58*	0.58	*1.96*	0.28	*1.86*	0.34	*2.47*
POC:SPM (%)	3.81	*1.39*	3.25	*1.28*	4.07	*1.44*	4.60	*1.40*	3.72	*1.31*
PON:SPM (%)	0.50	*1.46*	0.40	*1.28*	0.55	*1.49*	0.66	*1.49*	0.45	*1.31*
TEP:SPM (g XG eq./g)	0.054	*2.27*	0.033	*2.26*	0.066	*2.26*	0.067	*2.27*	0.071	*1.62*
LoI (%)	22.9	*1.37*	17.0	*1.38*	25.5	*1.36*	25.4	*1.26*	21.1	*1.27*
Dissolved parameters										
Salinity	31.6	*1.03*	31.7	*1.03*	30.6	*1.02*	31.8	*1.02*	32.5	*1.02*
DOC conc.(mg/l)	1.42	*1.32*	1.45	*1.46*	1.54	*1.25*	1.50	*1.20*	1.28	*1.22*
TDN conc. (µmol/l)	29.3	*1.54*	45.2	*1.29*	31.9	*1.51*	19.3	*1.25*	23.8	*1.26*
TDP conc. (µmol/l)	0.78	*1.42*	1.00	*1.27*	0.58	*1.42*	0.74	*1.15*	0.78	*1.41*
Si conc. (µmol/l)	11.08	*1.82*	18.5	*1.29*	9.81	*1.54*	4.54	*1.54*	14.0	*1.26*
Seabed parameters										
POC in sediment (%)	1.98	*0.18*	-	-	-	-	-	-	-	-
PON in sediment (%)	0.27	*0.02*	-	-	-	-	-	-	-	-

1012 **Table A.2**: idem Table A.1 but now for W05.

	year		winter		spring		summer		autumn	
	mean	std	mean	std	mean	std	mean	std	mean	std
Particulate parameters										
Hach Turbidity (FNU)	3.88	*2.87*	9.34	*1.79*	1.56	*3.15*	2.36	*1.81*	4.42	*2.51*
SPM-mass conc. (mg/l)	8.5	*1.82*	13.6	*1.67*	7.7	*1.64*	5.6	*1.55*	9.3	*1.75*
SPM-vol conc. (µl/l)	41	*1.82*	61	*1.98*	40	*1.77*	24	*1.08*	35	*1.47*
Median floc size (µm)	136	*1.51*	101	*1.40*	146	*1.20*	284	*1.03*	134	*1.43*
Effective floc density (mg/l)	47	*1.80*	71	*1.88*	45	*1.74*	26	*1.07*	40	*1.46*
POC conc. (mg/l)	0.56	*1.61*	0.52	*1.60*	0.83	*1.61*	0.39	*1.32*	0.49	*1.27*
PON conc. (mg/l)	0.074	*1.47*	0.067	*1.61*	0.094	*1.34*	0.071	*1.34*	0.072	*1.14*
TEP conc. (mg XG eq./l)	0.94	*1.84*	0.83	*2.14*	1.65	*1.55*	1.02	*1.41*	0.75	*1.61*
Chl-a conc. (µg/l)	3.03	*2.23*	1.46	*1.49*	4.82	*3.02*	3.62	*1.90*	3.88	*1.22*
Pheo-a conc. (µg/l)	0.14	*2.67*	0.10	*1.76*	0.13	*2.30*	0.19	*4.87*	0.15	*1.33*
POC:SPM (%)	6.74	*1.76*	3.80	*1.26*	10.84	*1.45*	9.52	*1.69*	7.21	*1.47*
PON:SPM (%)	0.93	*1.83*	0.49	*1.22*	1.45	*1.34*	1.46	*1.71*	1.13	*1.58*
TEP:SPM (g XG eq./g)	0.124	*2.08*	0.077	*2.07*	0.253	*1.49*	0.153	*1.52*	0.111	*2.01*
LoI (%)	40.6	*1.48*	26.2	*1.18*	54.0	*1.58*	57.5	*1.29*	36.8	*1.22*
Dissolved parameters										
Salinity	33.8	*1.02*	33.7	*1.03*	32.9	*1.03*	33.8	*1.03*	34.3	*1.01*
DOC conc.(mg/l)	1.10	*1.34*	1.08	*1.53*	1.52	*1.20*	1.07	*1.23*	1.01	*1.18*
TDN conc. (µmol/l)	14.7	*1.72*	25.5	*1.44*	18.2	*1.18*	9.5	*1.62*	12.4	*1.54*
TDP conc. (µmol/l)	0.48	*1.47*	0.69	*1.26*	0.47	*1.17*	0.37	*1.29*	0.44	*1.52*
Si conc. (µmol/l)	4.48	*1.90*	7.72	*2.07*	4.10	*1.22*	2.30	*1.56*	4.68	*1.50*
Seabed parameters										
POC in sediment (%)	1.80	*0.28*	-	-	-	-	-	-	-	-
PON in sediment (%)	0.26	*0.03*	-	-	-	-	-	-	-	-

1013

1014 **Table A.3**: idem Table A.1 but now for W08.

	year		winter		spring		summer		autumn	
	mean	std	mean	std	mean	std	mean	std	mean	std
Particulate parameters										
Hach Turbidity (FNU)	1.74	*1.93*	2.44	*1.94*	0.98	*1.64*	1.16	*1.94*	2.03	*1.46*
SPM-mass conc. (mg/l)	3.72	*1.46*	4.74	*1.36*	3.48	*1.30*	2.74	*1.47*	3.96	*1.28*
SPM-vol conc. (µl/l)	23	*1.84*	39	*1.57*	15	*1.32*	11	*1.13*	21	*1.55*
Median floc size (µm)	148	*1.44*	119	*1.21*	175	*1.08*	187	*1.04*	162	*1.70*
Effective floc density (mg/l)	27	*1.77*	44	*1.50*	17	*1.30*	13	*1.12*	23	*1.50*
POC conc. (mg/l)	0.32	*1.42*	0.26	*1.38*	0.45	*1.24*	0.33	*1.45*	0.37	*1.21*
PON conc. (mg/l)	0.045	*1.43*	0.038	*1.47*	0.057	*1.28*	0.045	*1.30*	0.053	*1.26*
TEP conc. (mg XG eq./l)	0.62	*1.66*	0.32	*1.54*	0.79	*1.21*	0.58	*1.59*	0.81	*1.46*
Chl-a conc. (µg/l)	1.00	*1.53*	1.09	*1.49*	0.63	*1.37*	0.80	*1.48*	1.33	*1.26*
Pheo-a conc. (µg/l)	0.044	*1.50*	0.044	*1.44*	-	-	0.029	*1.54*	0.056	*1.27*
POC:SPM (%)	8.71	*1.70*	5.56	*1.43*	13.05	*1.20*	13.63	*1.58*	9.34	*1.37*
POC:SPM (%)	1.20	*1.77*	0.77	*1.54*	1.65	*1.30*	2.17	*1.53*	1.42	*1.39*
TEP:SPM (g XG eq./g)	0.169	*1.85*	0.075	*1.52*	0.226	*1.29*	0.173	*1.82*	0.21	*1.64*
LoI (%)	40.2	*1.44*	28.9	*1.36*	74.9	*1.11*	49.5	*1.21*	38.0	*1.34*
Dissolved parameters										
Salinity	34.94	*1.004*	34.98	*1.004*	34.76	*1.002*	34.91	*1.006*	34.96	*1.002*
DOC conc.(mg/l)	0.96	*1.35*	1.09	*1.53*	1.02	*1.09*	0.98	*1.26*	0.82	*1.13*
TDN conc. (µmol/l)	8.3	*1.67*	15.3	*1.28*	6.13	*1.18*	5.4	*1.54*	7.3	*1.25*
TDP conc. (µmol/l)	0.33	*1.59*	0.59	*1.31*	0.24	*1.15*	0.23	*1.15*	0.27	*1.38*
Si conc. (µmol/l)	2.53	*1.58*	3.60	*1.37*	1.99	*1.12*	1.89	*1.60*	2.44	*1.51*
Seabed parameters										
POC in sediment (%)	1.09	*0.38*	-	-	-	-	-	-	-	-
PON in sediment (%)	0.19	*0.08*	-	-	-	-	-	-	-	-

1015

Appendix B: Monthly Model Parameters for TEP:SPM model

Table B.1: Monthly model parameters for TEP. The units for K_{POM} are mg/l (POC, PON) and mg XG eq./l (TEP) and for f_1 and f_2 [g/(g POM)] for POC and PON and in [g XG eq./(g POM)] for TEP. For the monthly fits three months are combined, centered around the month of interest.

m_{POM}=0.13	K_{POM} CI 95% [lower, upper]	f_1 CI 95% [lower, upper]	f_2 CI 95% [lower, upper]
January	4.25 [2.68, 6.00]	0.098 [0.059, 0.153]	0.251 [0.186, 0.319]
February	2.37 [1.66, 3.61]	0.078 [0.006, 0.198]	0.656 [0.465, 0.845]
March	1.91 [1.82, 1.99]	0.971 [0.583, 1.200]	0.444 [0.173, 0.793]
April	3.67 [2.12, 4.83]	0.489 [0.386, 0.641]	0.457 [0.265, 0.677]
May	4.96 [2.24, 7.11]	0.476 [0.386, 0.722]	0.090 [0.022, 0.154]
June	4.69 [2.58, 6.54]	0.412 [0.305, 0.576]	0.136 [0.065, 0.235]
July	4.78 [3.11, 6.80]	0.312 [0.233, 0.426]	0.297 [0.150, 0.531]
August	2.68 [1.03, 4.32]	0.371 [0.226, 0.714]	0.540 [0.392, 0.695]
September	1.91 [1.73, 2.10]	0.387 [0.285, 0.400]	0.526 [0.414, 0.653]
October	1.77 [1.56, 1.95]	0.291 [0.183, 0.435]	0.499 [0.406, 0.518]
November	1.99 [1.90, 2.13]	0.138 [0.058, 0.235]	0.346 [0.263, 0.441]
December	2.50 [1.46, 3.67]	0.081 [0.027, 0.147]	0.314 0.251, 0.383[]

Appendix C: C:N Ratio

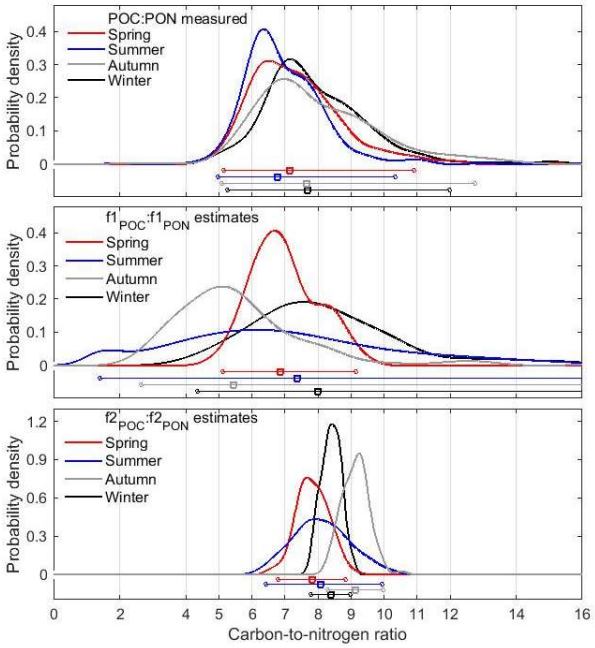

Figure C.1: Probability density distribution of the POC:PON ratio from in situ measurements and of the Carbon to Nitrogen ratios of the model parameters f_1(POC):f_1(PON) and f_2(POC):f_2(PON). The horizontal bars are the 95% CI.

Appendix D: Carbon Content of the TEP

Engel and Passow (2001) have reported that the carbon concentration of the TEP (mg/l) is linearly correlated with the TEP concentration (in (mg XG eq.)/l). The conversion factor between both depends on the chemical composition of the TEP and ranges from about 0.51 to 0.88 (mg/ (mg XG eq.)). The slope of this regression line can be estimated by the POC:TEP ratio. The ratio derived from the measured POC and TEP concentrations is about 1 for all data, lower values are found in summer (0.64) and autumn (0.80) and higher ones in spring (2.08) and winter (1.28). Clearly, only the summer and autumn values are realistic and within the range reported by Engel and Passow (2001). The ratios derived from the POM:SPM model have a lower variability than those from the measurements. The fresh POC over fresh TEP ratio is approaching a constant value at SPM concentration above about 50 mg/l, whereas the ratio POC:TEP for the mineral-associated fraction (also derived from the POM:SPM model) is constant. The ratio for the fresh POC and fresh TEP is on average about 0.50 (spring), 0.38 (summer), 0.87 (autumn) and 0.45 (winter), corresponding with an overall slope factor of 0.55±0.22. Similarly, the mineral-associated POC over TEP ratio for spring is 0.52, for summer 0.63, for autumn 0.54 and for winter 1.04 (on average 0.68±0.24). If all the POC is TEP, then these ratios provide an upper limit of the C content of fresh TEP. It is remarkable that the differences between fresh and mineral-associated ratios are small and that, notwithstanding the large uncertainties associated with the ratios (see Figures 5-7), the values of the slope factor derived from the model agree with the estimates from Engel and Passow (2001). The overall conversion of TEP concentration into carbon TEP concentration based on the model estimates is: C-TEP (mg/l) = 0.57±0.21 TEP (mg XG eq./l).

References

Adriaens, R., Zeelmaekers, E., Fettweis, M., Vanlierde, E., Vanlede, J., Stassen, P., et al. (2018). Quantitative clay mineralogy as provenance indicator for recent muds in the southern North Sea. *Marine Geology*, 398, 48-58. https://doi.org/10.1016/j.margeo.2017.12.011

Agrawal, Y., & Pottsmith, H. (2000). Instruments for particle size and settling velocity observations in sediment transport. *Marine Geology*, 168, 89–114. https://doi.org/10.1016/S0025-3227(00)00044-X

Alldredge, A.L., Passow, U., & Logan, B.E. (1993). The abundance and significance of a class of large, transparent organic particles in the ocean. *Deep-Sea Research*, 40,1131–1140. https://doi.org/10.1016/0967-0637(93)90129-Q

Andrews, S., Nover, D., & Schladow, S. (2010). Using laser diffraction data to obtain accurate particle size distributions: The role of particle composition. *Limnology and Oceanography Methods*, 8, 507–526. https://doi.org/10.4319/lom.2010.8.507

Arndt, S., Jørgensen, B.B., LaRowe, D.E., Middelburg, J.J., Pancost, R.D., & Regnier, P. (2013). Quantifying the degradation of organic matter in marine sediments: A review and synthesis. *Earth-Science Reviews*, 123, 53-86. https://doi.org/10.1016/j.earscirev.2013.02.008

Baeteman, C., Scott, D.B., & Van Strydonck, M. (2002). Changes in coastal zone processes at a high sea-level stand: a late-Holocene example from Belgium. *Journal of Quaternary Science*, 17, 547–559. https://doi.org/10.1002/jqs.707

Baeye, M., & Fettweis, M. (2015). In situ observations of suspended particulate matter plumes at an offshore wind farm. *Geo-Marine Letters*, 35, 247-255. https://doi.org/10.1007/s00367-015-0404-8

Beardsley, R.C., Limeburner, R., & Rosenfeld, L.K. (1985). Introduction to CODE-2 Moored Array and Large-Scale Data Report. Woods Hole Oceanogr. Inst. Techn. Rep. WHOI-85-35, CODE Technical Report No 38, 234 pp.

Bhaskar, P.V., & Bhosle, N.B. (2006). Dynamics of transparent exopolymeric particles (TEP) and particle-associated carbohydrates in the Dona Paula bay, west coast of India. Journal of Earth System Science, 115**,** 403–413. https://doi.org/10.1007/BF02702869

Blattmann, T.M., Liu, Z., Zhang, Y., Zhao, Y., Haghipour, N., Montluçon, D.B., et al. (2019). Mineralogical control on the fate of continentally derived organic matter in the ocean. *Science*, 366, 742–745. https://doi.org/10.1126/science.aax5345

Bouillon, S., Yambélé, A., Spencer, R.G.M., Gillikin, D.P., Hernes, P.J., Six, J., et al. (2012). Organic matter sources, fluxes and greenhouse gas exchange in the Oubangui River (Congo River basin). *Biogeosciences*, 9, 2045–2062, https://doi.org/10.5194/bg-9-2045-2012

Braithwaite, K., Bowers, D., Nimmo-Smith, W., & Graham, G. (2012). Controls on floc growth in an energetic tidal channel. *Journal of Geophysical Research Oceans*, 117, C02024. https://doi.org/10.1029/2011JC007094

Buonassissi, C.J., & Dierssen, H.M. (2010). A regional comparison of particle size distributions and the power law approximation in oceanic and estuarine surface waters. *Journal of Geophysical Research Oceans*, 115, C10028. https://doi.org/10.1029/2010JC006256

1088 Capuzzo, E., Lynam, C.P., Barry, J., Stephens, D., Forster, R.M., Greenwood, N., et al. (2018).
1089 A decline in primary production in the North Sea over 25 years, associated with reductions in
1090 zooplankton abundance and fish stock recruitment. *Global Change Biology*, 24, e352–e364.
1091 https://doi.org/10.1111/gcb.13916

1092 Capuzzo, E., Stephens, D., Silva, T., Barry, J., & Forster, R.M. (2015). Decrease in water clarity
1093 of the southern and central North Sea during the 20th century. *Global Change Biology*, 21,
1094 2206–2214. https://doi.org/10.1111/gcb.12854

1095 Chen, Y., Wang, M., Zhou, X., Fu, H., Qu, X., & Zhu, D. (2021). Sorption fractionation of
1096 bacterial extracellular polymeric substances (EPS) on mineral surfaces and associated effects on
1097 phenanthrene sorption to EPS-mineral complexes. *Chemosphere*, 263, 128264.
1098 https://doi.org/10.1016/j.chemosphere.2020.128264

1099 Chowdhury, C., Majumder, N., & Jana, T.K. (2016). Seasonal distribution and correlates of
1100 transparent exopolymer particles (TEP) in the waters surrounding mangroves in the Sundarbans.
1101 *Journal of Sea Research*, 112, 65-74. http://doi.org/10.1016/j.seares.2016.01.004

1102 Cross, J., Nimmo-Smith, W.A.M., Torres, R., & Hosegood, P.J. (2013). Biological controls on
1103 resuspension and the relationship between particle size and the Kolmogorov length scale in a
1104 shallow coastal sea. *Marine Geology*, 343, 29-38. https://doi.org/10.1016/j.margeo.2013.06.014

1105 Davies, E.J., Nimmo-Smith, W.A.M., Agrawal, Y.C., & Souza, A.J. (2012). LISST-100 response
1106 to large particles. *Marine Geology*, 307-310, 117–122.
1107 https://doi.org/10.1016/j.margeo.2012.03.006

1108 Decho, A. W., & Gutierrez, T. (2017). Microbial extracellular polymeric substances (EPSs) in
1109 ocean systems. *Frontiers in Microbiology*, 8 (922). https://doi.org/10.3389/fmicb.2017.00922

1110 Deng, Z., He, Q., Safar, Z., & Chassagne, C. (2019). The role of algae in fine sediment
1111 flocculation: In-situ and laboratory measurements. *Marine Geology*, 413, 71–84.
1112 https://doi.org/10.1016/j.margeo.2019.02.003

1113 Desmit, X., Nohe, A., Borges, A.V., Prins, T., De Cauwer, K., Lagring, R., et al. (2020).
1114 Changes in chlorophyll concentration and phenology in the North Sea in relation to de-
1115 eutrophication and sea surface warming. *Limnology and Oceanography*, 65, 828–847.
1116 https://doi.org/10.1002/lno.11351

1117 Desmit, X., Thieu, V., Billen, G., Campuzano, F., Dulière, V., Garnier, J., et al. (2018).
1118 Reducing marine eutrophication may require a paradigmatic change. *Science of the Total*
1119 *Environment*, 635, 444–1466. https://doi.org/10.1016/j.scitotenv.2018.04.181

1120 Doerffer, R., & Schiller, H. (2007). The MERIS Case 2 water algorithm. *International Journal of*
1121 *Remote Sensing*, *28*, 517-535. https://doi.org/10.1080/01431160600821127

1122 Droppo, I.G. (2001). Rethinking what constitutes suspended sediment. Hydrol. Process. 15,
1123 1551–1564. https://doi.org/10.1002/hyp.228

1124 Dyer, K.R. (1989). Sediment processes in estuaries: Future research requirements. *Journal of*
1125 *Geophysical Research Oceans*, 94, 14327-14339. https://doi.org/10.1029/JC094iC10p14327

1126 Eisma, D., & Kalf, J. (1979). Distribution and particle size of suspended matter in the Southern
1127 Bight of the North Sea and the eastern Channel. *Netherlands Journal of Sea Research,* 13, 298-
1128 304. https://doi.org/10.1016/0077-7579(79)90008-5

1129 Engel, A., Endres, S., Galgani, L., & Schartau, M. (2020). Marvelous marine microgels: On the
1130 distribution and impact of gel-like particles in the oceanic water-column. *Frontiers in Marine*
1131 *Science*, 7, 405. https://doi.org/10.3389/fmars.2020.00405

1132 Engel, A., & Passow, U. (2001). Carbon and nitrogen content of transparent exopolymer
1133 particles (TEP) in relation to their Alcian Blue adsorption. *Marine Ecology Progress Series*, 219,
1134 1-10. doi:10.3354/meps219001

1135 Engel, A., & Schartau, M. (1999). Influence of transparent exopolymer particles (TEP) on
1136 sinking velocity of Nitzschia closterum aggregates. *Marine Ecology Progress Series*, 182, 69-76.
1137 doi:10.3354/meps182069

1138 Etcheber, H., Taillez, A., Abril, G., Garnier, J., Servais, P., Moatar, F., & Commarieu, M.-V.
1139 (2007). Particulate organic carbon in the estuarine turbidity maxima of the Gironde, Loire and
1140 Seine estuaries: origin and lability. *Hydrobiology*, 588, 245-259. https://doi.org/10.1007/s10750-
1141 007-0667-9

1142 EUMETSAT (2019). Sentinel-3 Product Notice - OLCI level-2 Ocean Colour, EUM/OPS-
1143 SEN3/TEN/19/1068317

1144 Fall, K.A., Friedrichs, C.T., Massey, G.M., Bowers, D.G., & Smith, J.S. (2021). The importance
1145 of organic content to fractal floc properties in estuarine surface waters: Insights from video,
1146 LISST, and pump sampling. *Journal of Geophysical Research Oceans,* 126, e2020JC016787.
1147 https://doi.org/10.1029/2020JC016787

1148 Fettweis, M., & Baeye, M. (2015). Seasonal variation in concentration, size and settling velocity
1149 of muddy marine flocs in the benthic boundary layer. *Journal of Geophysical Research Oceans*,
1150 120, 5648-5667. https://doi.org/10.1002/2014JC010644

1151 Fettweis, M., Baeye, M., Van der Zande, D., Van den Eynde, D., & Lee, B.J. (2014). Seasonality
1152 of floc strength in the southern North Sea. *Journal of Geophysical Research Oceans*, 119, 1911–
1153 1926. https://doi.org/10.1002/2013JC009750

1154 Fettweis, M., Francken, F., Pison, V., & Van den Eynde, D. (2006). Suspended particulate matter
1155 dynamics and aggregate sizes in a high turbidity area. *Marine Geology*, 235, 63-74.
1156 https://doi.org/10.1016/j.margeo.2006.10.005

1157 Fettweis, M., & Lee, B.J. (2017). Spatial and seasonal variation of biomineral suspended
1158 particulate matter properties in high-turbid nearshore and low-turbid offshore zones. *Water*, 9,
1159 694. https://doi.org/10.3390/w9090694

1160 Fettweis, M., Monbaliu, J., Nechad, B., Baeye, M., & Van den Eynde D. (2012). Weather and
1161 climate related spatial variability of high turbidity areas in the North Sea and the English
1162 Channel. *Methods in Oceanography*, 3-4, 25-39. https://doi.org/10.1016/j.mio.2012.11.001

1163 Fettweis, M., Riethmüller, R., Verney, R., Becker, M., Backers, J., Baeye, M., et al. (2019).
1164 Uncertainties associated with in situ long-term observations of suspended particulate matter
1165 concentration using optical and acoustic sensors. *Progress in Oceanography*, 178, 102162.
1166 https://doi.org/10.1016/j.pocean.2019.102162

1167 Fettweis, M., & Van den Eynde, D. (2003). The mud deposits and the high turbidity in the
1168 Belgian–Dutch coastal zone, southern bight of the North Sea. *Continental Shelf Research,* 23,
1169 669–691. https://doi.org/10.1016/S0278-4343(03)00027-X

1170 Frigstad, H., Andersen, T., Hessen, D.O., Naustvoll, L.-J., Johnsen, T.M., & Bellerby, R.G.J.
1171 (2011). Seasonal variation in marine C:N:P stoichiometry: Can the composition of seston explain
1172 stable Redfield ratios? *Biogeosciences*, 8, 2917–2933. https://doi.org/10.5194/bg-8-2917-2011

1173 Fuchs, E., Zimmerman, R.C., & Jaffe, J.S. (2002). The effect of elevated levels of phaeophytin in
1174 natural water on variable fluorescence measured from phytoplankton. *Journal of Plankton*
1175 *Research*, 24, 1221-1229. https://doi.org/10.1093/plankt/24.11.1221

1176 Fukao, T., Kimoto, K., & Kotani, Y. (2010). Production of transparent exopolymer particles by
1177 four diatom species. *Fisheries Science*, 76, 755–760. https://doi.org/10.1007/s12562-010-0265-z

1178 Hemingway, G.D., Rothman, D.H., Grant, K.E., Rosengard, S.Z., Eglinton, T.I., Derry L.A., &
1179 Galy V.V. (2019). Mineral protection regulates long-term global preservation of natural organic
1180 carbon. *Nature*, 570, 228-238. https://doi.org/10.1038/s41586-019-1280-6

1181 Hendriks, H.C.M., van Prooijen, B.C., Aarninkhof, S.G.J., & Winterwerp, J.C. (2020). How
1182 human activities affect the fine sediment distribution in the Dutch Coastal Zone seabed.
1183 *Geomorphology*, 367, 107314. https://doi.org/10.1016/j.geomorph.2020.107314

1184 Høyer, J.L., & Karagali, I. (2016). Sea surface temperature climate data record for the North Sea
1185 and Baltic Sea. *Journal of Climate*, 29, 2529–2541. https://doi.org/10.1175/JCLI-D-15-0663.1

1186 Ittekkot, V., & Laane, R.W.P.M. (1991). Fate of riverine particulate organic matter. In:
1187 Biogeochemistry of Major World Rivers (Degens, E.T., Kempe, S., Richey, R., eds). SCOPE 42.
1188 Wiley and Sons, New York, 233–242.

1189 Jachlewski, S., Jachlewski, W.D., Linne, U., Brasen, C., Wingender, J., & Siebers, B. (2015).
1190 Isolation of extracellular polymeric substances from biofilms of the thermoacidophilic archaeon
1191 Sulfolobus acidocaldarius. *Frontiers in Bioengineering and Biotechnology*, 3, 123.
1192 https://doi.org/10.3389/fbioe.2015.00123

1193 Jago, C.F., Bale, A.J., Green, M.O., Howarth, M.J., Jones, S.E., McCave, I.N., et al. (1994).
1194 Resuspension processes and seston dynamics, southern North Sea. In: Understanding the North
1195 Sea System (Charnock, H., Dyer, K.R., Huthnance, J.M., Liss, P.S., Simpson, J.H., Tett, P.B.,
1196 eds.), Springer Verlag. https://doi.org/10.1007/978-94-011-1236-9_8

1197 Jago, C.F., Kennaway, G.M., Novarino, G., & Jones, S.E. (2007). Size and settling velocity of
1198 suspended flocs during a phaeocystis bloom in the tidally stirred Irish Sea, NW European Shelf.
1199 *Marine Ecology Progress Series*, 345, 51–62, doi:10.3354/meps07006.

1200 Jaiser, R., Dethloff, K., Handorf, D., Rinke, H., & Cohen, J. (2012). Impact of sea ice cover
1201 changes on the Northern Hemisphere atmospheric winter circulation. *Tellus A*, 64, 11595.
1202 https://doi.org/10.3402/tellusa.v64i0.11595

1203 Johnston, R.J., & Semple, R.K. (1983). Classification using information statistics. In: Concepts
1204 and Techniques in Modern Geography, 37, GeoBooks, Norwich, UK, 43pp.

1205 Kalbitz, K., Schwesig, D., Rethemaeyer, J., & Matzner, E. (2005). Stabilization of dissolved
1206 organic matter by sorption to the mineral soil. *Soil Biology and Biochemistry*, 37, 1319-1331.
1207 https://doi.org/10.1016/j.soilbio.2004.11.028

1208 Keil, R.G., Montluçon, D.B., Prahl, F.G., & Hedges, J.I. (1994). Sorptive preservation of labile
1209 organic matter in marine sediments. *Nature*, 370, 549-552. https://doi.org/10.1038/370549a0

1210 Keyvani, A., & Strom, K. (2014) Influence of cycles of high and low turbulent shear on the
1211 growth rate and equilibrium size of mud flocs. *Marine Geology*, 354, 1-14.
1212 https://doi.org/10.1016/j.margeo.2014.04.010

1213 Lacroix, G., Ruddick, K., Ozer, J., & Lancelot, C. (2004). Modelling the impact of the Scheldt
1214 and Rhine/Meuse plumes on the salinity distribution in Belgian waters (southern North Sea).
1215 *Journal of Sea Research*, 52, 149– 163. https://doi.org/10.1016/j.seares.2004.01.003

1216 Lai, H., Fang, H., Huang, L., He, G., & Reible, D. (2014). A review on sediment bioflocculation:
1217 Dynamics, influencing factors and modeling. *Science of the Total Environment*, 642, 1184–1200.
1218 https://doi.org/10.1016/j.scitotenv.2018.06.101

1219 Lancelot, C., Spitz, Y., Gypens, N., Ruddick, K., Becquevort, S., Rousseau, V., et al. (2005).
1220 Modelling diatom and Phaeocystis blooms and nutrient cycles in the Southern Bight of the North
1221 Sea: The MIRO model. *Marine Ecology Progress Series*, 289: 63–78. doi:10.3354/meps289063

1222 Lavigne, H., Van der Zande, D., Ruddick, K., Dos Santos, J.C., Gohin, F., Brotas, V., & Kratzer,
1223 S., 2021. Quality-control tests for OC4, OC5 and NIR-red satellite chlorophyll-a algorithms
1224 applied to coastal waters. *Remote Sensing of Environment*, 112237.
1225 https://doi.org/10.1016/j.rse.2020.112237

1226 Lee, B.J., Fettweis, M., Toorman, E., & Molz, F.J. (2012). Multimodality of a particle size
1227 distribution of cohesive suspended particulate matters in a coastal zone. *Journal of Geophysical*
1228 *Research Oceans*, 117, C03014. https://doi.org/10.1029/2011JC007552

1229 Lee, B.J., Kim, J., Hur, J., Choi, I-H., Toorman, E., Fettweis, M., & Choi, J.W. (2019) Seasonal
1230 dynamics of organic matter composition and its effects on suspended sediment flocculation in
1231 river water. *Water Resources Research*, 55, 6968-6985. https://doi.org/10.1029/2018WR024486

1232 Lee, J.H., Lee, W.C., Kim, H.C., Jo, N., Jang, H.K., Kang, J.J., et al. (2020). Transparent
1233 Exopolymer Particle (TEPs) Dynamics and Contribution to Particulate Organic Carbon. *Water*,
1234 12, 1057; https://doi.org/10.3390/w12041057

1235 Liénart, C., Savoye, N., Bozec, Y., Breton, E., Conan, P., David, V., et al. (2017). Dynamics of
1236 particulate organic matter composition in coastal systems: A spatio-temporal study at multi-
1237 systems scale. *Progress in Oceanography*, 156, 221–239.
1238 https://doi.org/10.1016/j.pocean.2017.03.001

1239 Liley, J.B. (1992). Fitting size distributions to optical particle counter data. *Aerosol Science and*
1240 *Technology*, 17, 84-92. https://doi.org/10.1080/02786829208959562

1241 Logan, B.E., Passow, U., Alldredge, A.L., & Grossarts, S.M. (1995). Rapid formation and
1242 sedimentation of large aggregates is predictable from coagulation rates (half-lives) of transparent
1243 exopolymer particles (TEP). *Deep-Sea Research II*, 42, 203-214. https://doi.org/10.1016/0967-
1244 0645(95)00012-F

1245 Long, R.A., & Azam, F. (1996). Abundant protein-containing particles in the sea. *Aquatic*
1246 *Microbial Ecology*, 10, 213-221. doi:10.3354/ame010213

1247 Maerz, J., Hofmeister, R., van der Lee, E.M., Gräwe, U., Riethmüller, R., & Wirtz, K.W. (2016).
1248 Maximum sinking velocities of suspended particulate matter in a coastal transition zone.
1249 *Biogeosciences*, 13, 4863–4876. https://doi.org/10.5194/bg-13-4863-2016

1250 Maggi, F. (2009). Biological flocculation of suspended particles in nutrient-rich aqueous
1251 ecosystems. *Journal of Hydrology*, 376, 116–125. https://doi.org/10.1016/j.jhydrol.2009.07.040

1252 Maggi, F., & Tang, F.H.M. (2015). Analysis of the effect of organic matter content on the
1253 architecture and sinking of sediment aggregates. *Marine Geology*, 363, 102–111.
1254 https://doi.org/10.1016/j.margeo.2015.01.017

1255 Malpezzi, M.A., Sanford, L.P., & Crump, B.C. (2013). Abundance and distribution of
1256 transparent exopolymer particles in the estuarine turbidity maximum of Chesapeake Bay. *Marine*
1257 *Ecology Progress Series*, 486, 23–35. https://doi.org/10.3354/meps10362

1258 Manning, A.J., Van Kessel, T., Melotte, J., Sas, M., Winterwerp, H., & Pidduck, E.L. (2011). On
1259 the consequence of a new tidal dock on the sedimentation regime in the Antwerpen area of the
1260 Lower Sea Scheldt. *Continental Shelf Research*, 31, S150-S164.
1261 https://doi.org/10.1016/j.csr.2010.10.008

1262 Mari. X., & Burd, A. (1998). Seasonal size spectra of transparent exopolymeric particles (TEP)
1263 in a coastal sea and comparison with those predicted using coagulation theory. *Marine Ecology*
1264 *Progress Series*, 163, 63-76. doi:10.3354/meps171063

1265 Mari, X., Passow, U., Migon, C., Burd, A.B., & Legendre, L. (2017). Transparent exopolymer
1266 particles: Effects on carbon cycling in the ocean. *Progress in Oceanography*, 151,13-37.
1267 https://doi.org/10.1016/j.pocean.2016.11.002

1268 Mari, X., & Robert, M. (2008). Metal induced variations of TEP sticking properties in the
1269 southwestern lagoon of New Caledonia. *Marine Chemistry*, 110, 98-108.
1270 https://doi.org/10.1016/j.marchem.2008.02.012

1271 Mari, X., Rochelle-Newall, E., Torréton, J.-P., Pringault, O., Jouon, A., & Migon, C. (2007).
1272 Water residence time: A regulatory factor of the DOM to POM transfer efficiency. *Limnology*
1273 *and Oceanography*, 52, 808–819. https://doi.org/10.4319/lo.2007.52.2.0808

1274 May, C.L., Koseff, J.R., Lucas, L.V., Cloern, J.E., & Schoellhamer, D.H. (2003). Effects of
1275 spatial and temporal variability of turbidity on phytoplankton blooms. *Marine Ecology Progress*
1276 *Series*, 254, 111-128. doi:10.3354/meps254111

1277 Mayer, L.M. (1994). Relationships between mineral surfaces and organic carbon concentrations
1278 in soils and sediments. *Chemical Geology*, 114, 347-363. https://doi.org/10.1016/0009-
1279 2541(94)90063-9

1280 Mietta, F., Chassagne, C., Manning, A.J., & Winterwerp, J.C. (2009). Influence of shear rate,
1281 organic matter content, pH and salinity on mud flocculation. *Ocean Dynamics*, 59, 751–763.
1282 https://doi.org/10.1007/s10236-009-0231-4

1283 Mikkelsen, O., Curran, K., Hill, P., & Milligan, T. (2007). Entropy analysis of in situ particle
1284 size spectra, *Estuarine Coastal and Shelf Science*, 72, 615–625.
1285 https://doi.org/10.1016/j.csr.2006.11.004

1286 Mikkelsen, O., Hill, P., & Milligan, T. (2006). Single-grain, microfloc and macrofloc volume
1287 variations observed with a LISST-100 and a digital floc camera. *Journal of Sea Research*, 55,
1288 87–102. https://doi.org/10.1016/j.seares.2005.09.003

1289 Milliman, J.D., Quichun, X., & Zuosheng, Y. (1984). Transfer of particulate organic carbon and
1290 nitrogen from Yangtze river to the Ocean. *American Journal of Science*, 284, 824-835.
1291 https://doi.org/10.2475/ajs.284.7.824

1292 Milliman, J.D., Yun-Shan, Q., Mei-E, R., & Saito, Y (1987). Man's influence on the erosion and
1293 transport of sediment by Asian rivers: The yellow river (Huanghe) example. *Journal of Geology*,
1294 95, 751-762. https://doi.org/10.1086/629175

1295 Morelle, J., Schapira, M., Françoise, S., Courtay, G., Orvain, F., & Claquin, P. (2018). Dynamics
1296 of exopolymeric carbon pools in relation with phytoplankton succession along the salinity
1297 gradient of a temperate estuary (France). *Estuarine Coastal and Shelf Science*, 209, 18-29.
1298 https://doi.org/10.1016/j.ecss.2018.05.008

1299 Muylaert, K., Gonzales, R., Franck, M., Lionard, M., Van der Zee, C., Cattrijsse, A., et al.
1300 (2006). Spatial variation in phytoplankton dynamics in the Belgian coastal zone of the North Sea
1301 studied by microscopy, HPLC-CHEMTAX and underway fluorescence recordings. *Journal of*
1302 *Sea Research*, 55, 253–265. https://doi.org/10.1016/j.seares.2005.12.002

1303 Neukermans, G., Ruddick, K., Loisel, H., & Roose, P. (2012). Optimization and quality control
1304 of suspended particulate matter concentration measurement using turbidity measurements.
1305 *Limnology and Oceanography Methods*, 10, 1011–1023.
1306 https://doi.org/10.4319/lom.2012.10.1011

1307 Neumann, A., Hass, H.C., Möbius, J., & Naderipour, C. (2019). Ballasted flocs capture pelagic
1308 primary production and alter the local sediment characteristics in the coastal German Bight
1309 (North Sea). *Geosciences*, 9, 344. https://doi.org/10.3390/geosciences9080344

1310 Nohe, A., Goffin, A., Tyberghein, L., Lagring, R., De Cauwer, K., Vyverman, W., & Sabbe, K.
1311 (2020). Marked changes in diatom and dinoflagellate biomass, composition and seasonality in
1312 the Belgian Part of the North Sea between the 1970s and 2000s. *Science of the Total*
1313 *Environment*, 716, 136316. https://doi.org/10.1016/j.scitotenv.2019.136316

1314 Nosaka, Y., Yamashita, Y., & Suzuki, K. (2017). Dynamics and origin of Transparent
1315 Exopolymer Particles in the Oyashio region of the Western Subarctic Pacific during the spring
1316 diatom bloom. *Frontiers in Marine Science*, 4, 79. https://doi.org/10.3389/fmars.2017.00079

1317 Ortega-Retuerta, E., Marrasé, C., Muñoz-Fernández, A., Sala, M.M., Simó, R., & Gasol, J.M.
1318 (2018). Seasonal dynamics of transparent exopolymer particles (TEP) and their drivers in the
1319 coastal NW Mediterranean Sea. *Science of the Total Environment*, 631–632, 180-190.
1320 https://doi.org/10.1016/j.scitotenv.2018.02.341

1321 Passow, U. (2000). Formation of transparent exopolymer particles, TEP, from dissolved
1322 precursor material. *Marine Ecology Progress Series*, 192, 1-11. doi:10.3354/meps192001

1323 Passow, U. (2002). Transparent exopolymer particles (TEP) in aquatic environments. *Progress*
1324 *in Oceanography*, 55, 287–333. https://doi.org/10.1016/S0079-6611(02)00138-6

1325 Passow, U., & Alldredge, A.L. (1995). A dye-binding assay for the spectrophotometric
1326 measurement of transparent exopolymer particles. *Limnology and Oceanography*, 40, 1326–
1327 1335. https://doi.org/10.4319/lo.1995.40.7.1326

Pietrzak, J.D., de Boer, G.J., & Eleveld, M.A. (2011). Mechanisms controlling the intra-annual mesoscale variability of SST and SPM in the southern North Sea. *Continental Shelf Research*, 31, 594–610. https://doi.org/10.1016/j.csr.2010.12.014

Ramaiah, N., Yoshikawa, T., & Furuya, K. (2001). Temporal variations in transparent exopolymer particles (TEP) associated with a diatom springbloom in a subarctic ria in Japan. *Marine Ecology Progress Series*, 212, 79-88. doi:10.3354/meps212079

Regnier, P., Friedlingstein, P., Ciais, P. Mackenzie, F.T., Gruber, N., Janssens, I.A., et al. (2013). Anthropogenic perturbation of the carbon fluxes from land to ocean. *Nature Geoscience*, 6, 597–607. https://doi.org/10.1038/ngeo1830

Röttgers, R., Heymann, K., & Krasemann, H. (2014). Suspended matter concentrations in coastal waters: methodological improvements to quantify individual measurement uncertainty. *Estuarine, Coastal and Shelf Science*, 151, 148–155. https://doi.org/10.1016/j.ecss.2014.10.010

Rousseau, V., Leynaert, A., Daoud, N., & Lancelot, C. (2002). Diatom succession, silicification and silicic acid availability in Belgian coastal waters (southern North Sea). *Marine Ecology Progress Series*, 236, 61–73. doi:10.3354/meps236061

Schartau, M., Engel, A., Schröter, J., Thoms, S., Völker, C., & Wolf-Gladrow, D. (2007). Modelling carbon overconsumption and the formation of extracellular particulate organic carbon. *Biogeosciences*, 4, 433–454. https://doi.org/10.5194/bg-4-433-2007

Schartau, M., Riethmüller, R., Flöser, G., van Beusekom, J.E.E., Krasemann, H., Hofmeister, R., & Wirtz, K. (2019). On the separation between inorganic and organic fractions of suspended matter in a marine coastal environment. *Progress in Oceanography*, 171, 231-250. https://doi.org/10.1016/j.pocean.2018.12.011

Schlünz, B., & Schneider, R.R. (2000). Transport of terrestrial organic carbon to the oceans by rivers: Re-estimating flux- and burial rates. *International Journal of Earth Science*, 88, 599-606. https://doi.org/10.1007/s005310050290

Schwarz, C., Cox, T.J.S., Van Engeland, T., Van Oevelen, D., Van Belzen, J., van de Koppel, J., et al. (2017). Field estimates of floc dynamics and settling velocities in a tidal creek with significant along-channel gradients in velocity and SPM. *Estuarine, Coastal and Shelf Science*, 197, 221-235. https://doi.org/10.1016/j.ecss.2017.08.041

Shen, X., Toorman, E.A., Lee, B.J., & Fettweis, M. (2018). Biophysical flocculation of suspended particulate matters in Belgian coastal zones. *Journal of Hydrology*, 567, 238-252. https://doi.org/10.1016/j.jhydrol.2018.10.028

Shen, X., Toorman, E.A., Lee, B.J., & Fettweis, M. (2019). An approach to modeling biofilm growth during the flocculation of suspended cohesive sediments. *Journal of Geophysical Research Ocean*, 124, 4098-4116. https://doi.org/10.1029/2018JC014493

Skinnebach, K.H., Fruergaard, M., & Andersen, T.A. (2020). Biological effects on flocculation of fine-grained suspended sediment in natural seawater. *Estuarine, Coastal and Shelf Science*, 228, 106395. https://doi.org/10.1016/j.ecss.2019.106395

Smith, D.C., Simon, M., Alldredge, A.L., & Azam, F. (1992). Intense hydrolytic enzyme activity on marine aggregates and implications for rapid particle dissolution. *Nature*, 359, 139–141. https://doi.org/10.1038/359139a0

1369 Stavn, R.H., Rick, H.J., & Falster, A.V. (2009). Correcting the errors from variable sea salt
1370 retention and water of hydration in loss on ignition analysis: Implications for studies of estuarine
1371 and coastal waters. *Estuarine, Coastal and Shelf Science*, 81, 575-582.
1372 https://doi.org/10.1016/j.ecss.2008.12.017

1373 Tang, F.H.M., & Maggi, F. (2016). A mesocosm experiment of suspended particulate matter
1374 dynamics in nutrient- and biomass-affected waters. *Water Research*, 89, 76–86.
1375 https://doi.org/10.1016/j.watres.2015.11.033

1376 Tran, D., & Strom, K. (2017). Suspended clays and silts: Are they independent or dependent
1377 fractions when it comes to settling in a turbulent suspension? *Continental Shelf Research*, 138,
1378 81-94. http://doi.org/10.1016/j.csr.2017.02.011

1379 Van Beusekom, J.E.E., Buschbaum, C., & Reise, K. (2012). Wadden Sea tidal basins and the
1380 mediating role of the North Sea in ecological processes: Scaling up of management? *Ocean &*
1381 *Coastal Management*, 68, 69–78, https://doi.org/10.1016/j.ocecoaman.2012.05.002

1382 Van Engeland, T., Soetaert, K., Knuijt, A., Laane, R.W.P.M., & Middelburg, J.J. (2010).
1383 Dissolved organic nitrogen dynamics in the North Sea: A time series analysis (1995–2005).
1384 *Estuarine, Coastal and Shelf Science*, 89, 31-42. https://doi.org/10.1016/j.ecss.2010.05.009

1385 Van Hoey, G., Vincx, M., & Degraer, S. (2005). Small- to large-scale geographical patterns
1386 within the macrobenthic Abra alba community. *Estuarine, Coastal and Shelf Science*, 64, 751-
1387 763. https://doi.org/10.1016/j.ecss.2005.03.022

1388 Van Maren, D.S., van Kessel, T., Cronin, K., & Sittoni, L. (2015). The impact of channel
1389 deepening and dredging on estuarine sediment concentration. *Continental Shelf Research*, 95, 1–
1390 14. https://doi.org/10.1016/j.csr.2014.12.010

1391 Verdugo, P. (2012). Marine microgels. *Annual Review of Marine Science*, 4, 375–400.
1392 https://doi.org/10.1146/annurev-marine-120709-142759

1393 Verney, R., Lafite, R., & Brun-Cottan, J. (2009). Flocculation potential of estuarine particles:
1394 The importance of environmental factors and of the spatial and seasonal variability of suspended
1395 particulate matter. *Estuaries and Coasts*, 32, 678–693. https://doi.org/10.1007/s12237-009-9160-
1396 1

1397 Wang, Y.P., Voulgaris, G., Li, Y., Yang, Y., Gao, J., Chen, J., & Gao, S. (2013). Sediment
1398 resuspension, flocculation, and settling in a macrotidal estuary. *Journal of Geophysical Research*
1399 *Oceans*, 118, 5591–5608. https://doi.org/10.1002/jgrc.20340

1400 Winterwerp, JC. (1998)., A simple model for turbulence induced flocculation of cohesive
1401 sediment. *Journal of Hydraulic Research*, 36, 309-326.
1402 https://doi.org/10.1080/00221689809498621

1403 Zhang, J., Liu, G., Wang, R., & Huang, H. (2017). Polycyclic aromatic hydrocarbons in the
1404 water-SPM-sediment system from the middle reaches of Huai River, China: Distribution,
1405 partitioning, origin tracing and ecological risk assessment. *Environmental Pollution*, 230, 61-71.
1406 https://doi.org/10.1016/j.envpol.2017.06.012

1407 Zhang, Y., Ren, J., Zhang, W., & Wu, J. (2021). Importance of salinity-induced stratification on
1408 flocculation in tidal estuaries. *Journal of Hydrology*, 596, 126063.
1409 https://doi.org/10.1016/j.jhydrol.2021.126063

1410 Zhou, J., Mopper, K., Passow, U., 1998. The role of surface-active carbohydrates in the
1411 formation of transparent exopolymer particles by bubble adsorption of seawater. *Limnology and*
1412 *Oceanography*, 43, 1860–1871. https://doi.org/10.4319/lo.1998.43.8.1860